Chemical Geology 320–321 (2012) 113–127

Contents lists available at SciVerse ScienceDirect

Chemical Geology

journal homepage: www.elsevier.com/locate/chemgeo

Research paper

Asthenospheric source of Neoproterozoic and Mesozoic kimberlites from the North Atlantic craton, West Greenland: New high-precision U–Pb and Sr–Nd isotope data on perovskite

Sebastian Tappe [a,*], Agnete Steenfelt [b], Troels Nielsen [b]

[a] Department of Earth and Atmospheric Sciences, University of Alberta, 1-26 Earth Sciences Building, Edmonton, Alberta, Canada T6G 2E3
[b] Geological Survey of Denmark and Greenland, Øster Voldgade 10, DK-1350, Copenhagen, Denmark

ARTICLE INFO

Article history:
Received 17 January 2012
Received in revised form 17 May 2012
Accepted 29 May 2012
Available online 5 June 2012

Editor: L. Reisberg

Keywords:
Mantle reservoirs
Redox melting
Kimberlite origin
Carbonatite evolution
Craton reactivation
ID-TIMS

ABSTRACT

We present combined U–Pb, Sr, and Nd isotope data for small perovskite crystal fractions from kimberlites in West Greenland. Based on this high-precision TIMS data set, we revise the age range for kimberlite magma emplacement in the Sarfartoq and Tikiusaaq fields to 550–590 Ma and 158–166 Ma, respectively. These improved U–Pb perovskite age constraints reinforce the close temporal association of kimberlite and carbonatite magmatism across the North Atlantic craton.

The new combined U–Pb, Sr, and Nd isotope data for perovskites provide evidence for kimberlite magma derivation from a moderately depleted mantle source region during both the Neoproterozoic and Mesozoic. Moreover, we demonstrate that the difference in initial Sr–Nd isotope compositions between the Neoproterozoic Sarfartoq ($^{87}Sr/^{86}Sr = 0.70278–0.70293$; $\varepsilon_{Nd} = +1.6$ to $+3.6$; $n = 13$) and Mesozoic Tikiusaaq ($^{87}Sr/^{86}Sr = 0.70319–0.70346$; $\varepsilon_{Nd} = +4.8$ to $+5.1$; $n = 3$) kimberlite fields can be readily explained by isotopic evolution of a common mantle reservoir. This mantle reservoir appears to have continuously participated in global crust–mantle differentiation and recycling, which points to the well-stirred convective upper mantle as the ultimate kimberlite magma source region beneath West Greenland. The apparent geographic shift of kimberlite and associated carbonatite magmatic activity from the craton margin during the Neoproterozoic toward the craton center during the Mesozoic is explained by changes in localized, small-scale mantle flow along the underside of progressively thinning cratonic lithosphere.

1. Introduction

High-precision geochronology and radiogenic isotope tracer analyses are vital tools for the study of magmatic processes. Their combination provides a powerful means to foster a better understanding of the relationships between magma generation and large-scale tectonic processes (Gibson et al., 2006; Tappe et al., 2007; Corfu and Dahlgren, 2008). It is now well established that the production of certain magma compositions relates to specific physicochemical conditions prevalent in the source region during melting and that these conditions are largely controlled by tectonic setting (Green et al., 1987; Pearce and Peate, 1995; Foley, 2011). However, some low-volume, deep-seated magma types such as kimberlites do not have straightforward relationships to geodynamic processes. For example, while some workers suggest a strong subduction influence in the genesis of kimberlites and related rocks (Sharp, 1974; Currie and Beaumont, 2011), others advocate a genetic link to mantle plumes (Le Roex, 1986; Haggerty, 1994; Torsvik et al., 2010; Rao and Lehmann, 2011) or continental rifting processes (Batumike et al., 2008; Tappe et al., 2008). In the study of kimberlite magma genesis it is therefore critical to combine geochronology and tracer isotope information to obtain further insight into the mechanism(s) responsible for the production of this economically important magma type.

Historically, Sr and Nd isotope compositions were instrumental in the recognition of the involvement of two distinct mantle reservoirs during Mesozoic kimberlite magmatism beneath southern Africa (Smith, 1983). These first isotope data for kimberlites, which led to the original Group-I and II subdivison, were collected on carefully selected whole-rock powders. However, it is now widely accepted that the high degree of scatter commonly observed in kimberlite isotope data is primarily due to secondary processes including crustal contamination (Paton et al., 2007; Woodhead et al., 2009; Tappe et al., 2011a). In an earlier attempt to circumvent this problem and to resolve small isotopic differences, Heaman (1989) analyzed the Sr and Nd isotope composition of the primary groundmass phase perovskite from a number of North American kimberlites by conventional ID-TIMS methods. He noted an overall decrease in data scatter and the less radiogenic $^{87}Sr/^{86}Sr$ of

* Corresponding author at: Institut für Mineralogie, Westfälische Wilhelms-Universität, Corrensstrasse 24, 48149 Münster, Germany. Tel.: +49 251 8333470; fax: +49 251 8338397.
E-mail address: sebastian.tappe@uni-muenster.de (S. Tappe).

0009-2541/$ – see front matter © 2012 Elsevier B.V. All rights reserved.
doi:10.1016/j.chemgeo.2012.05.026

kimberlitic perovskite compared to the corresponding bulk kimberlite (see also Paton et al., 2007). Furthermore, Heaman (1989) stressed the opportunity to add high-precision U–Pb ages (Kramers and Smith, 1983) to the same perovskite fractions for which the primary Sr and Nd isotope compositions were determined.

Here we present an application of combined U–Pb geochronology and Sr–Nd isotope analysis of perovskite to the petrogenesis of kimberlites from the North Atlantic craton (NAC) in West Greenland (Fig. 1). Based on these new high-precision data we will argue for a convective upper mantle origin of both Neoproterozoic and Mesozoic kimberlite magmatism beneath the NAC. The new data also enable us to place further constraints on the temporal and genetic relationships between kimberlite and carbonatite magmatism throughout the NAC.

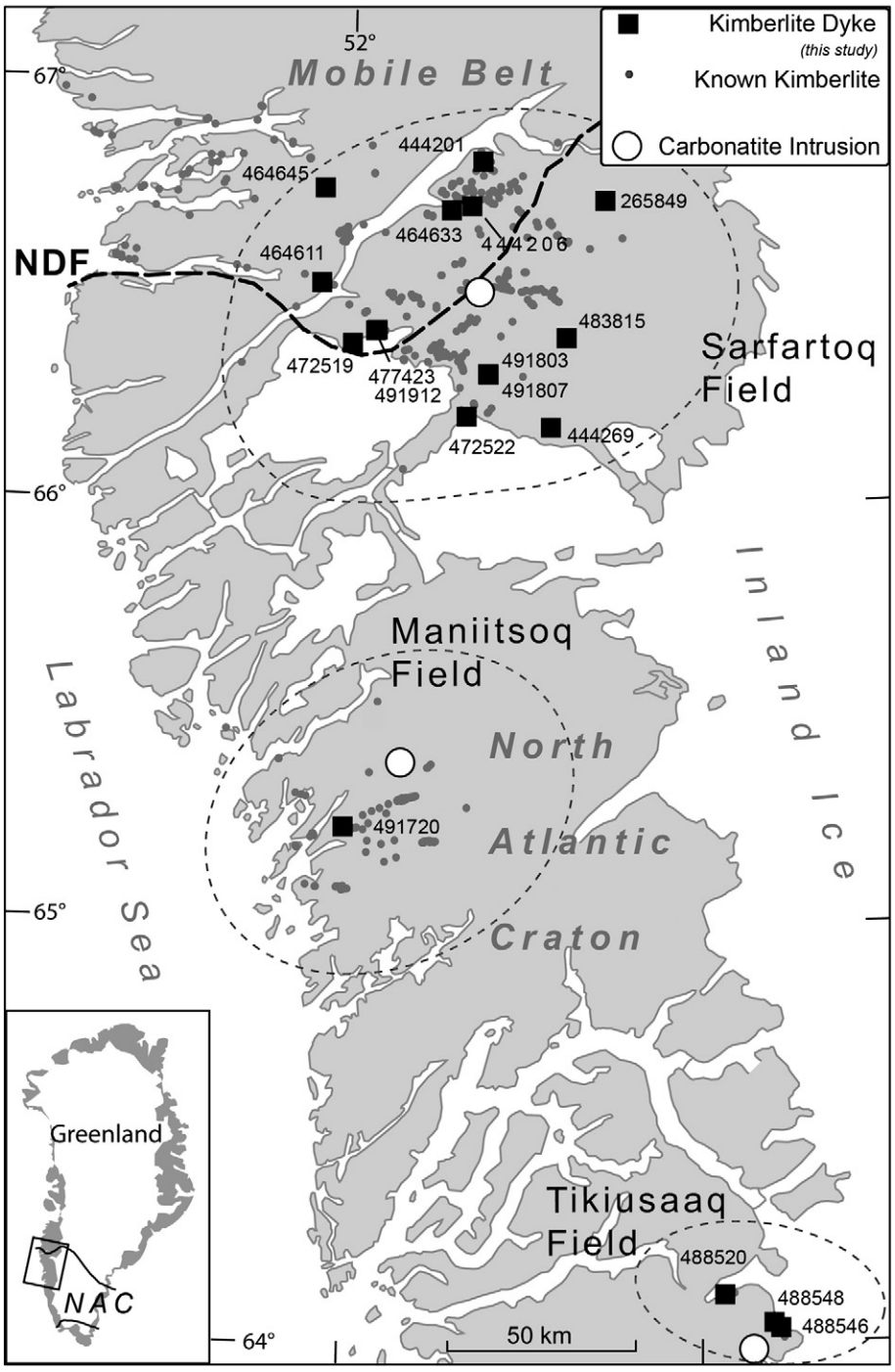

Fig. 1. Location of the Sarfartoq, Maniitsoq, and Tikiusaaq kimberlite fields in West Greenland. Note that the Neoproterozoic Sarfartoq kimberlite field at the margin and the Jurassic Tikiusaaq kimberlite field inside the North Atlantic craton (NAC) are both accompanied by similar old carbonatite intrusions (open circles; not to scale). Samples discussed in this paper (black squares) are superimposed over all known kimberlite and aillikite occurrences of the region (see Secher et al., 2009; also for more geochronology). The new combined U–Pb ages and Sr–Nd isotope compositions of perovskite from West Greenland kimberlite dykes are summarized in Tables 1 and 2, respectively. Geographic coordinates for the studied samples from Sarfartoq and Tikiusaaq are listed in Table 1. New U–Pb perovskite age and Sr–Nd isotope data for the Majuagaa kimberlite dyke segment 491720 (Maniitsoq field) are given in Tappe et al. (2011a). NDF — Nagssugtoqidian Deformation Front.

2. West Greenland kimberlite magmatism

2.1. Timing and possible tectonic settings

The North Atlantic craton (NAC) in West Greenland and Labrador has been a site of protracted volatile-rich ultramafic magmatism for almost 3 billion years. Summaries of the various magma types produced and their emplacement ages can be found in Larsen and Rex (1992), Tappe et al. (2007), and Secher et al. (2009). Magmatic activity of kimberlite affinity, however, was restricted to the Neoproterozoic (~600–550 Ma; Tappe et al., 2011a) and Jurassic (~200–150 Ma; Larsen et al., 2009), but there was only little spatial overlap between these two kimberlite events. Neoproterozoic kimberlite magmatism in West Greenland was confined to the northern part of the NAC (e.g., Sarfartoq and Maniitsoq fields), whereas the Jurassic kimberlite magmatic activity occurred further to the south (e.g., Tikiusaaq and Pyramidefjeld fields). Importantly, both Neoproterozoic and Jurassic kimberlite magmatism were associated with the intrusion of carbonatites (Larsen and Rex, 1992; Secher et al., 2009; Tappe et al., 2009; Tappe et al., 2011a).

The Neoproterozoic kimberlite and carbonatite magmatic activities on either side of the Labrador Sea have been variably interpreted as a consequence of far-field stresses related to the opening of the Iapetus Ocean (Larsen and Rex, 1992), incipient lithospheric thinning along an intra-cratonic deep fracture zone (Tappe et al., 2006, 2007), and impingement of a mantle plume (Tachibana et al., 2006; Ernst and Bell, 2010). The relationship between kimberlite magmatism and tectonic setting is more evident for the Jurassic occurrences in West Greenland. During the early Mesozoic, an extensive continental rift system developed, progressively cutting through the NAC (Chalmers and Pulvertaft, 2001; Keen et al., 2012). This rift system eventually split the NAC, opening a small ocean basin at ca. 60 Ma, which now forms the Labrador Sea. It therefore appears that the Jurassic kimberlite and carbonatite magmatism along the borders of the Labrador Sea represents the earliest manifestation of NAC break-up (Hansen, 1980; Tappe et al., 2007; Larsen et al., 2009; Tappe et al., 2009). Additional evidence for reactivation of the cratonic lithosphere in West Greenland during the Mesozoic comes from 'fossil' mantle peridotite-derived geotherms, which are much warmer during the Jurassic (>44 mW/m^2 beneath Pyramidefjeld; Hutchison et al., 2007) than during the Neoproterozoic (~38 mW/m^2 beneath Sarfartoq; Sand et al., 2009).

2.2. Samples analyzed

In this study we focus on a suite of Neoproterozoic kimberlites from the Sarfartoq area at the northern margin of the NAC, and a suite of Jurassic kimberlites from the Tikiusaaq area, located well inside the craton (Fig. 1). Although the diamondiferous dyke rocks investigated here are compositionally transitional between kimberlite and aillikite – *an ultramafic lamprophyre variety* – , we refer to these carbonate- and phlogopite-bearing ultramafic dykes collectively as kimberlites (the same applies to the Labrador occurrences). For a modern account of the observed petrographic variety within this kimberlite province the reader is referred to Nielsen et al. (2009) and Tappe et al. (2009). Furthermore, it is important to note that these kimberlites are associated with sizeable carbonatite intrusions at both Sarfartoq and Tikiusaaq (Fig. 1). For the purpose of this paper, we shall refer to these intrusive bodies at crustal levels as 'carbonatites' (or 'carbonatite magmas'), whereas we refer to CO_2-rich, SiO_2-poor melt compositions in the Earth's mantle as 'carbonate melts' (~40 wt.% CO_2; SiO_2<15 wt.%) and 'carbonate–silicate melts' (CO_2<25 wt.%; SiO_2>15 wt.%).

The first U–Pb perovskite results for the Sarfartoq kimberlite field have been reported in Secher et al. (2009) and for the Tikiusaaq field in Tappe et al. (2009). We have further improved age constraints and report here updated U–Pb perovskite age determinations for 14 kimberlite dykes from Sarfartoq (Fig. 2A) and 3 kimberlite dykes from Tikiusaaq (Fig. 2B). These revised U–Pb data (Table 1) will be discussed together with the newly determined Sr and Nd isotope compositions (Table 2), which have been obtained from the same perovskite fractions. It is the aim of the present study to track the ultimate kimberlite source region(s) beneath West Greenland through time by utilizing this combined analytical approach. In addition to the new isotope data, we provide a summary (Table 3) and compilation (Table A, Supplementary data file) of high-quality major and trace element analyses of Sarfartoq and Tikiusaaq kimberlites.

3. Analytical techniques

The analytical protocol for our combined U–Pb age and Sr–Nd isotope ratio determinations of perovskite has been reported in detail in Tappe and Simonetti (2012). Below we provide a summary of the analytical techniques employed during the study of perovskite from West Greenland kimberlites.

3.1. Perovskite from West Greenland kimberlites

Hand specimens of kimberlite dykes from the Sarfartoq (n = 14) and Tikiusaaq (n = 3) fields were processed through standard crushing and mineral separation procedures (e.g., Wilfley table, methylene iodide, Frantz isodynamic separator). The sample preparation techniques employed and first U–Pb results for these kimberlites are reported in Secher et al. (2009) and Tappe et al. (2009, 2011a). In general, perovskite recovery was best in the 80 to 120 μm range.

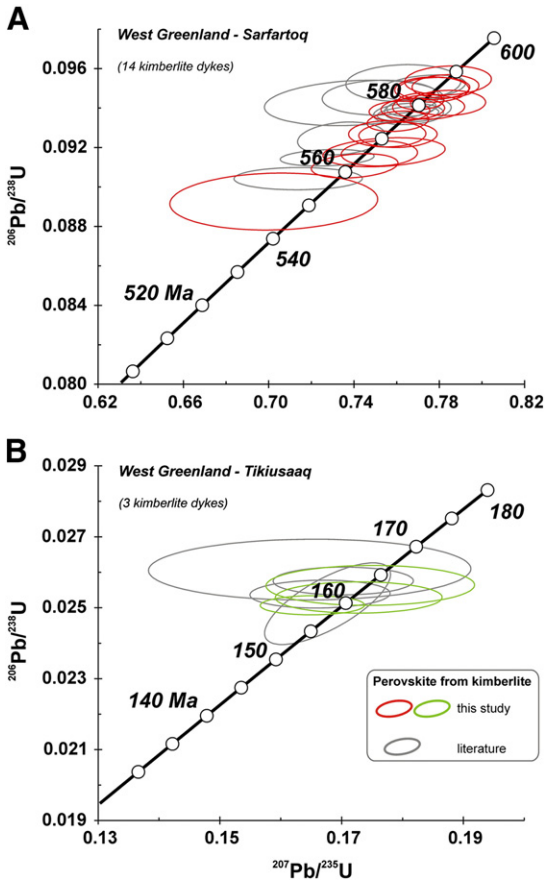

Fig. 2. U–Pb Concordia diagrams for perovskites from kimberlite dykes in (A) the Sarfartoq and (B) the Tikiusaaq area, West Greenland. The U–Pb data collected during this study (red and green ellipses) and previously published results from the same samples (gray ellipses; Secher et al., 2009; Tappe et al., 2009) have been used to calculate new Concordia ages (see Table 1). All analyses displayed are listed in Table 1 and the error ellipses are at the 2-sigma level of uncertainty.

Table 1
ID-TIMS U–Pb results for perovskite from Sarfartoq and Tikiusaaq kimberlite dykes, North Atlantic craton, West Greenland.

Description[a]	Longitude	Latitude	Weight (μg)	U (ppm)	Th (ppm)	Pb (ppm)	TCPb (pg)	$^{206}Pb/^{204}Pb$	$^{206}Pb/^{238}U$[b]	$^{207}Pb/^{235}U$[b]	$^{207}Pb/^{206}Pb$[b]	Apparent ages (Ma) $^{206}Pb/^{238}U$	$^{207}Pb/^{235}U$	$^{207}Pb/^{206}Pb$	Discordance [%]
West Greenland — Sarfartoq															
265849 (Concordia age = 585.8 ± 2.8 Ma; 2σ)	−50.478700	66.714510													
4. Brown fragments/octahedrons; M@0.6A (130)			59	92	454	23	195	184	0.09510 ± 24	0.7829 ± 64	0.05971 ± 50	585.6 ± 1.4	587.1 ± 3.6	593 ± 18	1.3
444201 (Concordia age = 566.0 ± 3.6 Ma; 2σ)	−51.214485	66.808650													
2. Black fragments; M@0.3A (200)			46	64	305	16	123	154	0.09176 ± 30	0.7541 ± 117	0.05961 ± 90	565.9 ± 1.8	570.6 ± 6.7	589 ± 32	4.1
444206 (WA Concordia age = 580.2 ± 1.5 Ma; 2σ)	−51.277233	66.702756													
1. Dark brown cubes; M@0.4A (209)[c]			92	203	982	48	467	262	0.09402 ± 18	0.7669 ± 47	0.05916 ± 36	579.2 ± 1.1	578.0 ± 2.7	573 ± 13	−1.1
3. Black-brown octahedrons; M@0.4A (50)			91	166	828	40	365	263	0.09434 ± 17	0.7711 ± 45	0.05928 ± 35	581.2 ± 1.0	580.4 ± 2.6	577 ± 13	−0.7
444269 (WA Concordia age = 570.9 ± 1.9 Ma; 2σ)	−50.809295	66.174839													
3. Dark brown fragments; M@0.6A (150)[c]			137	82	820	32	466	158	0.09246 ± 34	0.7341 ± 84	0.05758 ± 65	570.1 ± 2.0	559.0 ± 4.9	514 ± 25	−11.4
4. Dark brown fragments; M@0.6A (200)			136	81	1028	37	458	157	0.09264 ± 26	0.7606 ± 75	0.0595 ± 6	571.2 ± 1.5	574.3 ± 4.3	587 ± 22	2.8
5. Dark brown fragments; M@0.6A (100)			160	62	441	19	413	157	0.09269 ± 27	0.7556 ± 74	0.0591 ± 6	571.4 ± 1.6	571.5 ± 4.3	572 ± 22	0.1
464611 (Concordia age = 587.4 ± 3.5 Ma; 2σ)	−52.173025	66.517464													
4. Dark brown cubes; M@0.7A (200)			148	43	143	9	276	156	0.0954 ± 30	0.7841 ± 83	0.05961 ± 64	587.4 ± 1.7	587.8 ± 4.7	589 ± 23	0.4
464633 (WA Concordia age = 584.9 ± 1.7 Ma; 2σ)	−51.402072	66.691873													
2. Dark brown cubes; M@0.6A (100)[c]			105	62	811	28	233	180	0.09504 ± 26	0.7719 ± 83	0.05890 ± 60	585.3 ± 1.5	580.8 ± 4.8	563 ± 22	−4.1
4. Dark brown cubes; M@0.6A (100)			150	65	887	31	342	187	0.09499 ± 23	0.7774 ± 69	0.05936 ± 53	585.0 ± 1.4	584.0 ± 4.0	580 ± 19	−0.9
5. Dark brown cubes; M@0.6A (200)			298	59	954	33	699	167	0.09494 ± 26	0.7765 ± 71	0.05932 ± 56	584.7 ± 1.6	583.5 ± 4.1	579 ± 20	−1.0
464645 (WA Concordia age = 564.8 ± 1.8 Ma; 2σ)	−52.163320	66.743371													
2. Brown cubes; M@0.6A (150)[c]			60	49	174	10	119	164	0.09148 ± 17	0.7274 ± 90	0.05767 ± 70	564.3 ± 1.0	555.0 ± 5.3	517 ± 26	−9.5
3. Dark brown cubes; M@0.6A (200)			84	50	162	10	167	162	0.09170 ± 26	0.7519 ± 73	0.05947 ± 59	565.6 ± 1.5	569.3 ± 4.2	584 ± 21	3.4
472519 (Concordia age = 561.9 ± 3.0 Ma; 2σ)	−51.983543	66.374251													
2. Dark brown cubes; M@0.6A (250)			36	131	389	25	156	190	0.09107 ± 25	0.7403 ± 83	0.05895 ± 64	561.9 ± 1.5	562.6 ± 4.8	565 ± 24	0.6
472522 (WA Concordia age = 576.6 ± 1.6 Ma; 2σ)	−51.306065	66.201345													
1. Dark brown cubes; M@0.6A (100)[c]			83	78	301	17	174	228	0.09371 ± 15	0.7653 ± 59	0.05923 ± 44	577.4 ± 0.9	577.1 ± 3.4	576 ± 16	−0.3
3. Dark brown cubes; M@0.6A (200)			83	84	306	17	192	231	0.09333 ± 21	0.7606 ± 59	0.05911 ± 45	575.2 ± 1.2	574.4 ± 3.4	571 ± 17	−0.8
477423 (WA Concordia age = 577.9 ± 1.6 Ma; 2σ)	−51.848249	66.405014													
1. Dark brown cubes; M@0.5A (50)[c]			77	82	565	24	204	193	0.09370 ± 22	0.7655 ± 67	0.05925 ± 52	577.4 ± 1.3	577.2 ± 3.9	576 ± 19	−0.2
2. Black cubes; M@0.5A (150)[c]			146	69	415	19	341	194	0.09392 ± 25	0.7699 ± 64	0.05946 ± 49	578.7 ± 1.5	579.8 ± 3.7	584 ± 18	1.0
3. Black cubes; M@0.5A (200)			239	58	331	15	453	199	0.09384 ± 21	0.7613 ± 58	0.05884 ± 46	578.2 ± 1.3	574.8 ± 3.4	561 ± 17	−3.1
483815 (WA Concordia age = 556.7 ± 2.6 Ma; 2σ)	−50.714180	66.387985													
1. Dark brown octahedrons; M@0.4A (150)[c]			40	29	292	11	82	75.1	0.09042 ± 23	0.7138 ± 123	0.05726 ± 100	558.0 ± 1.3	547.0 ± 7.3	502 ± 38	−11.8
4. Black blocky fragments; M@0.4A (90)			54	31	363	15	168	73.3	0.08926 ± 59	0.7024 ± 199	0.05707 ± 163	551.1 ± 3.5	540.2 ± 11.8	494 ± 62	−12.0
491803 (Concordia age = 579.8 ± 2.8 Ma; 2σ)	−51.177030	66.301576													
3. Dark brown cubes; M@0.5A (200)			264	50	183	11	512	170	0.09405 ± 25	0.7750 ± 69	0.05976 ± 55	579.5 ± 1.5	582.6 ± 4.0	595 ± 20	2.7
491807 (WA Concordia age = 581.9 ± 1.3 Ma; 2σ)	−51.180900	66.301985													
2. Dark brown cubes; M@0.5A (150)[c]			261	49	186	11	509	168	0.09494 ± 89	0.7740 ± 10	0.05913 ± 55	584.7 ± 5.3	582.0 ± 5.8	572 ± 20	−2.4
3. Dark brown cubes/octahedrons; M@0.5A (200)			335	49	177	11	673	163	0.09426 ± 26	0.7841 ± 72	0.06033 ± 57	580.7 ± 1.5	587.8 ± 4.1	616 ± 20	5.9
491912 (WA Concordia age = 580.6 ± 3.5 Ma; 2σ)	−51.839667	66.405794													
1. Brown fragments; M@0.5A (120)[c]			125	26	220	9	242	133	0.09426 ± 47	0.7401 ± 172	0.05695 ± 130	580.7 ± 2.8	562.5 ± 10.0	490 ± 50	−19.5
2. Brown fragments; M@0.5A (150)[c]			94	23	142	7	128	122	0.09453 ± 36	0.7525 ± 112	0.05773 ± 87	582.3 ± 2.1	569.7 ± 6.5	520 ± 33	−12.6
3. Brown fragments; M@0.5A (150)[c]			91	22	135	7	118	123	0.09527 ± 38	0.7631 ± 110	0.05809 ± 85	586.6 ± 2.2	575.8 ± 6.3	533 ± 32	−10.5
4. Brown fragments; M@0.5A (200)			145	96	550	26	451	200	0.09396 ± 22	0.7676 ± 61	0.05925 ± 48	578.9 ± 1.3	578.4 ± 3.5	576 ± 17	−0.5

West Greenland — Tikiusaaq														
488520 (WA Concordia age = 159.4 ± 1.3 Ma; 2σ)	−49.873808	64.105810												
1. Brown octahedrons; IF0.4NM (80)[d]			189	214	1998	24	542	136	0.02511 ± 47	0.16764 ± 422	0.04842 ± 84	159.9 ± 3.0	157.4 ± 3.7	120 ± 40	−34.0
2. Brown cubes/octahedrons; IF0.4NM (250)			49	142	384	13	125	106	0.02507 ± 11	0.1652 ± 35	0.04780 ± 103	159.6 ± 0.7	155.3 ± 3.1	89 ± 50	−79.5
488546 (WA Concordia age = 162.1 ± 1.2 Ma; 2σ)	−49.573082	64.024570												
1. Brown octahedrons; MI-H (80)[d]			188	75	88	7	367	79.5	0.02538 ± 16	0.1664 ± 47	0.04755 ± 136	161.5 ± 1.0	156.3 ± 4.1	77 ± 67	−111.5
2. Brown octahedrons; MI-H (120)[d]			274	70	215	7	512	79.2	0.02575 ± 16	0.1702 ± 47	0.04795 ± 136	163.9 ± 1.0	159.6 ± 4.1	97 ± 66	−70.3
3. Brown cubes/octahedrons; MI-H (200)			45	61	286	5	81	72.5	0.02529 ± 18	0.1728 ± 56	0.04955 ± 164	161.0 ± 1.1	161.8 ± 4.9	174 ± 75	7.5
488548 (WA Concordia age = 163.8 ± 2.4 Ma; 2σ)	−49.608990	64.037060												
1. Brown octahedrons; MI-H (130)[d]			273	45	n.a.	6	713	46.4	0.02607 ± 35	0.1647 ± 108	0.04582 ± 305	165.9 ± 2.2	154.8 ± 9.3	infinite	infinite
2. Brown cubes/octahedrons; MI-H (200)			118	40	239	4	182	60.3	0.02563 ± 23	0.1747 ± 70	0.04943 ± 202	163.1 ± 1.4	163.5 ± 6.0	169 ± 93	3.2

Unless otherwise stated, all uncertainties in this table are quoted at 1-sigma; geographic coordinates are in decimal degrees using WGS84 datum (see Fig. 1 for location of samples); WA—weighted average.

[a] M@0.5A — perovskite grains selected from magnetic fraction at 0.5 A (Frantz); MI-H — perovskite grains selected from heavy mineral fraction after Methylene Iodide step; Numbers in parentheses correspond to numbers of fragments analyzed.

[b] Atomic ratios corrected for fractionation (0.105%/amu Pb and 0.123%/amu U), blank (6 pg Pb; 1 pg U), isotopic tracer, and initial common Pb (TCPb). Thorium concentrations calculated based on amount of ^{208}Pb present and $^{207}Pb/^{206}Pb$ model age; TCPb is estimated initial common Pb based on the Stacey and Kramers (1975) terrestrial Pb evolution model.

[c] Ages were cited in Secher et al. (2009), but no U–Pb data were reported (these are given here with permission from the author and GEUS).

[d] Results from Tappe et al. (2009).

Fresh cubes/octahedrons or fragments without visible inclusions were collected as morphologic fractions typically comprising more than 50 grains per fraction to obtain >30 μg aliquots.

3.2. U–Pb geochronology

The collected perovskite grains were washed repeatedly in warm 2N HNO_3 and Milli-Q water and then weighed on an UTM ultra-microbalance prior to transfer into 5 ml Savillex vials. Prior to sample dissolution in a 1:1 mixture of concentrated HF and HNO_3 on a hotplate at ~150 °C for at least 3 days, ^{235}U–^{205}Pb and ^{149}Sm–^{150}Nd tracer solutions were added to the perovskite/acid mix in order to determine U, Pb, Sm, and Nd concentrations by isotope dilution. Thorium concentrations were calculated based on the amount of common Pb corrected ^{208}Pb present and the $^{207}Pb/^{206}Pb$ model age.

Uranium and Pb were isolated from the perovskite sample solutions using HBr anion exchange chromatography (Bio-Rad AG 1-X8). The isotopic compositions of these elements were measured on a VG354 thermal ionization mass spectrometer using a Daly detector operated in analog mode. All isotopic data reported in Table 1 were corrected for mass discrimination (0.105%/amu Pb and 0.123%/amu U; determined using the long-term reproducibility of NBS 981 and NBS U500, respectively), tracer, and blank contribution (6 ± 0.5 pg Pb and 1.0 ± 0.1 pg U). The presence of initial common lead was corrected using the terrestrial lead evolution model of Stacey and Kramers (1975).

The perovskites analyzed during this study are concordant within analytical uncertainty and the $^{206}Pb/^{238}U$ ages are identical to the Concordia ages. The $^{206}Pb/^{238}U$ ages were shown in general to be more robust compared to $^{207}Pb/^{206}Pb$ and $^{207}Pb/^{235}U$ ages, because they are less sensitive to the initial common lead correction (Heaman, 1989; Wu et al., 2010). All age calculations and the plotting of results were performed with the Isoplot software (Ludwig, 2000) utilizing the recommended decay constants of $9.8485 * 10^{-10} a^{-1}$ for ^{235}U and $1.55125 * 10^{-10}\ a^{-1}$ for ^{238}U (Steiger and Jäger, 1977). All uncertainties are quoted at the 2-sigma level throughout the text.

3.3. Sr and Nd isotope ratio determinations

Subsequent to loading of the sample solutions onto the AG 1-X8 anion exchange resin as part of the U–Pb chemistry, the resin bed was washed with approximately 1.5 ml of 3.1 N HCl. This washout was collected and dried down for Sr and (Sm)–Nd separations, which were conducted on miniaturized resin beds of Eichrom Sr-Spec and Ln-Spec, respectively. Strontium isotopic analyses were performed using a Micromass Sector-54 thermal ionization mass spectrometer operating in static mode (single Re filaments). All Sr isotope analyses are corrected for mass fractionation using an exponential law and $^{86}Sr/^{88}Sr = 0.1194$. NIST SRM 987 yielded an average value for $^{87}Sr/^{86}Sr$ of 0.710233 ± 8 (2σ S.D. for 57 measurements) during the measurement period (November 2009 to December 2010) and all measured Sr isotopic ratios are reported relative to a value of 0.710249 for NIST SRM 987 (Thirlwall, 1991).

The Nd isotopic composition was analyzed by plasma ionization multi-collector mass spectrometry (MC-ICP-MS) on a *Nu* plasma multi-collector ICP-MS instrument in static mode and all isotope ratios were corrected with an exponential fractionation law using $^{146}Nd/^{144}Nd = 0.7219$. The in-house Alfa Nd isotope standard (200 ppb solution) was run repeatedly during the analytical sessions with a mean for $^{143}Nd/^{144}Nd$ of 0.512284 ± 23 (2σ S.D. for 17 measurements). This is in good agreement with the 7-year long-term average of 0.512255 ± 48 (2σ S.D. for 394 measurements) and all measured Nd isotopic ratios are reported relative to a value of 0.512265 for the Alfa standard. The average $^{143}Nd/^{144}Nd$ for the JNdi-1 standard, which was run as a secondary standard, yielded 0.512091 ± 8 (2σ S.D. for 5 measurements). This value overlaps with the 1-year average of 0.512104 ± 27 (2σ S.D. for 22 measurements) and is in

Table 2
Sr and Nd isotope compositions of perovskite from Sarfartoq and Tikiusaaq kimberlite dykes, North Atlantic craton, West Greenland.

Sample no.	ID-TIMS U–Pb age (Ma) (This study)	$^{87}Sr/^{86}Sr_m$	Sm (ppm)	Nd (ppm)	$^{147}Sm/^{144}Nd_m$	$^{143}Nd/^{144}Nd_m$	[a]$^{143}Nd/^{144}Nd_i$	[b]$(\varepsilon_{Nd})_i$
West Greenland — Sarfartoq								
265849-4	585.8 ± 2.8	0.702877 (23)	418	3997	0.0635	0.512254 (9)	0.512010	2.5
444201-2	566.0 ± 3.6	0.702911 (79)	375	2820	0.0808	0.512343 (8)	0.512044	2.6
444201-3	566.0 ± 3.6	0.702891 (17)	406	2937	0.0839	0.512339 (11)	0.512028	2.3
444206-3	580.2 ± 1.5	0.702820 (14)	219	2095	0.0635	0.512232 (7)	0.511991	2.0
444269-4	570.9 ± 1.9	0.703161 (17)	497	4213	0.0716	0.512245 (15)	0.511977	1.5
444269-5	570.9 ± 1.9	0.703153 (20)	419	3494	0.0728	0.512230 (13)	0.511958	1.1
464611-1	587.4 ± 3.5	0.702838 (27)	135	988	0.0829	0.512331 (14)	0.512012	2.6
464633-4	584.9 ± 1.7	0.702815 (13)	416	3963	0.0637	0.512222 (11)	0.511978	1.8
464633-5	584.9 ± 1.7	0.702781 (11)	216	2088	0.0627	0.512221 (7)	0.511981	1.9
464633-5-replicate	584.9 ± 1.7	0.702787 (12)	216	2086	0.0627	0.512205 (7)	0.511964	1.6
464645-3	564.8 ± 1.8	0.702905 (17)	159	1161	0.0832	0.512331 (17)	0.512023	2.2
472519-2	561.9 ± 3.0	0.702927 (17)	394	2864	0.0835	0.512342 (13)	0.512035	2.4
472522-3	576.6 ± 1.6	0.702837 (14)	288	2366	0.0740	0.512258 (8)	0.511979	1.6
477423-3	577.9 ± 1.6	0.702885 (17)	260	2042	0.0772	0.512306 (8)	0.512014	2.4
483815-4	556.7 ± 2.6	0.702876 (15)	175	1512	0.0703	0.512360 (63)	0.512103	3.6
491803-3	579.8 ± 2.8	0.702813 (15)	178	1360	0.0796	0.512305 (9)	0.512003	2.2
491807-3	581.9 ± 1.3	0.702784 (13)	190	1451	0.0793	0.512296 (6)	0.511994	2.1
491912-4	580.6 ± 3.5	0.702832 (17)	141	977	0.0876	0.512367 (7)	0.512034	2.8
West Greenland — Tikiusaaq								
488520-2	159.4 ± 1.3	0.703456 (12)	529	5995	0.0535	0.512736 (7)	0.512680	4.8
488546-3	162.1 ± 1.2	0.703370 (20)	355	4493	0.0480	0.512734 (10)	0.512683	5.0
488548-2	163.8 ± 2.4	0.703192 (13)	181	2274	0.0483	0.512738 (6)	0.512686	5.1

Sr isotope compositions were determined by TIMS and Nd isotope compositions in solution mode by isotope dilution MC-ICP-MS. Measured Sr and Nd isotope ratios are normalized to the following standard values: NBS987 = $^{87}Sr/^{86}Sr$ value of 0.710249 (Thirlwall, 1991); ALFA = $^{143}Nd/^{144}Nd$ value of 0.512265, equivalent to a La Jolla $^{143}Nd/^{144}Nd$ value of 0.51185.
Numbers in parentheses are 2-sigma-of-the-mean uncertainties for individual isotope ratio measurements.
[a] Initial isotope ratios calculated for the improved U–Pb ages for West Greenland kimberlites (see Table 1).
[b] Calculated using ^{147}Sm decay constant of $6.54 * 10^{-12} a^{-1}$ (Lugmair and Marti, 1978); $(^{143}Nd/^{144}Nd)_{CHUR} = 0.512638$ (Goldstein et al., 1984); $(^{147}Sm/^{144}Nd)_{CHUR} = 0.1967$ (Jacobsen and Wasserburg, 1980).

agreement with the recommended value of 0.512107 (Tanaka et al., 2000), which is equivalent to a La Jolla $^{143}Nd/^{144}Nd$ value of 0.511850. Procedural blanks of <60 pg Sr and <30 pg Nd are considered negligible, given that several nanograms of Sr and Nd were recovered from individual perovskite fractions.

4. Results

4.1. U–Pb systematics

The TIMS U–Pb results for perovskite from Sarfartoq and Tikiusaaq kimberlite dykes are listed in Table 1 and displayed in Figs. 2 and 3. We calculated weighted average Concordia ages for 9 (out of 14) investigated kimberlite dykes from Sarfartoq. These age calculations include all data from this study at the University of Alberta and the reproducible data for perovskite fractions from Secher et al. (2009). The age results reported in Secher et al. (2009) had been made commercially available to the Geological Survey of Denmark and Greenland through Geospec Consultants Limited in Edmonton utilizing the same analytical facility at the University of Alberta. For the remaining 5 (out of 14) kimberlite dyke samples from Sarfartoq, none of the U–Pb ages reported in Secher et al. (2009) were reproducible, and these data are therefore not included in Table 1. These perovskite fractions have a higher degree of U–Pb discordancy and typically contain a higher proportion of common Pb compared to our new data. For these kimberlite samples we therefore calculated Concordia ages from our newly determined concordant U–Pb data only, and these new age determinations are recommended here to supersede any previously reported dates.

All new and previous U–Pb perovskite analyses that are included here in age calculations (see Table 1, where the original numbering system is retained to enable identification of excluded perovskite fractions) are shown in the Concordia diagram in Fig. 2A in order to demonstrate that we only consider concordant data. The most important result from this reinvestigation, which corroborates only 6 out of 14 kimberlite dyke ages, is that the known age range for kimberlite magmatism in the Sarfartoq area appears to shrink from ~550–605 Ma to ~550–590 Ma (Figs. 2A–3A). This ~40 Myr time span of kimberlite/carbonatite magmatic activity at Sarfartoq is coeval with the timing of kimberlite/carbonatite magma emplacement at Aillik Bay in Labrador between ~555 and 590 Ma (Tappe et al., 2006). These two occurrences form part of the same Late Neoproterozoic kimberlite and alkaline magmatic province hosted by the once-contiguous NAC on either side of the Labrador Sea (see Section 2.1.).

We also calculated new Concordia ages for 3 kimberlite dykes from the Tikiusaaq field (Table 1) using perovskite fractions from this study and the previously analyzed fractions from Tappe et al. (2009). Figs. 2B and 3B illustrate the improved precision of the new U–Pb analyses, which fall within the analytical uncertainties of the published data. Consequently, the uncertainty of each weighted average age drops significantly (Fig. 3B), and we here revise the emplacement ages for kimberlite dykes 488520, 488546 and 488548 to 159.4 ± 1.3 Ma (previously 159.9 ± 6.0 Ma), 162.1 ± 1.2 Ma (previously 162.7 ± 1.4 Ma) and 163.8 ± 2.4 Ma (previously 165.9 ± 4.4 Ma), respectively (Table 1). This improved age resolution now enables us to better constrain the likely petrogenetic relationship between the ~158–166 Ma old kimberlite dykes and the ~155–160 Ma old carbonatite sheets at Tikiusaaq (cf., Tappe et al., 2009; see Section 5.1.).

4.2. Sr and Nd isotope compositions

Perovskites from the 550–590 Ma old Sarfartoq kimberlites show a relatively small range in measured $^{87}Sr/^{86}Sr$ between 0.70278 and 0.70293 (16 analyses for 13 kimberlite dykes; Table 2; Fig. 4). Only sample 444269 falls outside this narrow range and the two analyzed perovskite fractions yielded indistinguishable $^{87}Sr/^{86}Sr$ ratios of 0.70315 ± 2 and 0.70316 ± 2. This sample shows the lowest initial ε_{Nd} values of + 1.1 and + 1.5 compared with the majority of Sarfartoq

Table 3
Average major (wt.%) and trace element (ppm) concentrations of kimberlite dykes from West Greenland.

	Sarfartoq kimberlites ($n=27$)			Tikiusaaq kimberlites ($n=13$)		
	Average	Min	Max	Average	Min	Max
SiO_2	27.4	18.4	32.8	24.9	16.3	32.5
TiO_2	2.54	1.46	4.33	3.74	2.86	4.43
Al_2O_3	1.92	1.17	3.96	2.52	1.83	3.76
$Fe_2O_3^T$	13.1	10.4	21.2	14.4	13.0	17.3
MnO	0.21	0.16	0.35	0.23	0.16	0.33
MgO	27.9	17.7	35.4	19.5	12.9	28.0
CaO	10.8	2.6	22.8	18.5	10.3	27.1
Na_2O	0.07	0.00	0.34	0.13	0.08	0.22
K_2O	1.15	0.20	2.87	1.27	0.86	2.12
P_2O_5	0.62	0.07	1.87	0.90	0.34	1.74
LOI	14.5	10.5	20.0	13.1	6.6	20.3
CO_2	8.3	4.9	13.0	9.2	4.2	17.0
Total	100.2	98.6	101.6	99.3	99.1	99.4
LFSE						
Cs	1.0	0.2	3.6	0.5	0.3	0.8
Rb	50.5	13.4	119.0	48.3	29.6	87.4
Ba	768	312	1432	922	346	1670
Sr	1038	236	2408	2075	974	3947
HFSE						
Th	11.5	4.4	29.9	19.5	8.3	48.9
U	2.9	0.9	5.8	4.9	2.0	10.9
Nb	144	81	315	217	106	505
Ta	11.1	6.9	20.8	11.8	8.7	20.4
Pb	4.5	2.1	9.4	5.0	1.7	8.7
Zr	215	66	633	553	179	1023
Hf	5.4	1.7	16.6	12.9	4.7	23.4
Y	11.1	5.1	18.9	30.0	11.3	63.6
REE						
La	103.8	50.6	200.7	206.0	87.2	462.0
Ce	203.2	104.8	371.4	482.0	206.9	1052.6
Pr	23.0	11.5	40.4	49.5	22.2	111.8
Nd	88.0	45.3	166.6	179.7	80.6	415.6
Sm	11.5	6.1	21.3	23.3	11.0	50.7
Eu	2.99	1.63	5.40	5.99	2.73	12.94
Gd	7.57	3.77	13.16	14.54	6.74	31.58
Tb	0.78	0.40	1.38	2.00	0.92	4.40
Dy	3.21	1.65	5.61	7.83	3.43	16.84
Ho	0.46	0.22	0.79	1.05	0.42	2.23
Er	0.92	0.42	1.77	2.40	0.85	5.01
Tm	0.10	0.04	0.18	0.29	0.10	0.63
Yb	0.51	0.20	1.02	1.55	0.53	3.20
Lu	0.07	0.03	0.16	0.20	0.09	0.42
TM						
Cr	1391	546	1937	782	21	1553
Co	93	81	108	78	49	105
Ni	1044	325	1750	583	61	1246
Sc	17	5	42	20	13	29
V	157	79	226	230	148	351
Cu	91	37	148	101	68	121
Zn	82	61	136	90	63	152

Major and trace element concentrations are XRF and ICP-MS data, respectively. $Fe_2O_3^T$ = total Fe as ferric iron. LFSE = low field strength elements; HFSE = high field strength elements; REE = rare earth elements; TM = transition metals. The complete data set is provided in Table A of the Supplementary data file. Data sources for Sarfartoq: Gaffney et al. (2007) and Tappe et al. (2011a). Data source for Tikiusaaq: Steenfelt et al. (2007).

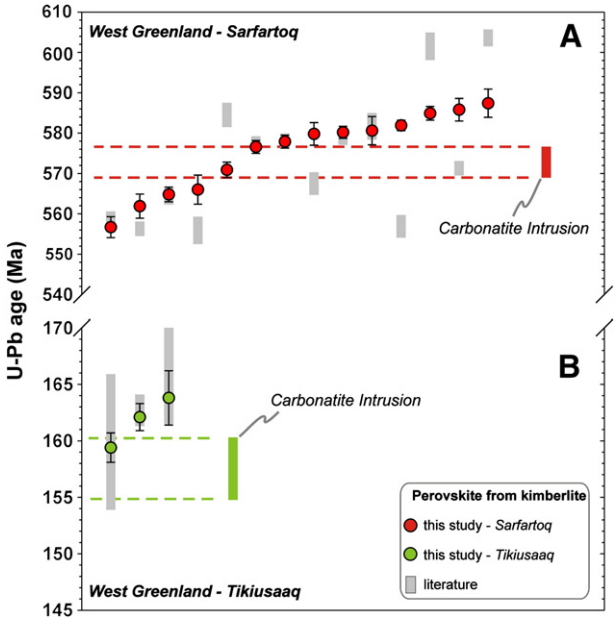

Fig. 3. Summary of U–Pb perovskite age results for (A) Sarfartoq and (B) Tikiusaaq kimberlites obtained during this study (see Table 1). The light gray bars in the backdrop represent the previous U–Pb perovskite ages for the same mineral separates (data for Sarfartoq from Secher et al., 2009 and for Tikiusaaq from Tappe et al., 2009). The currently most robust age for the Sarfartoq carbonatite intrusion is 572.8 ± 3.8 Ma (Tappe et al., 2011a) and shown here as the red bar and dashed lines in (A). The current best estimate for emplacement of the Tikiusaaq carbonatite intrusion is shown as green bar and dashed lines in (B), and it is based on high-precision TIMS U–Pb baddeleyite and pyrochlore, as well as TIMS Rb–Sr phlogopite data (Tappe et al., 2009). Error bars are at the 2-sigma level of uncertainty. See main text for more details.

kimberlitic perovskites (+1.6 to +3.6), which testifies to its isotopically more enriched nature (Fig. 4). In Fig. 4 the new Sr–Nd isotope data for perovskites from Sarfartoq are compared with corresponding whole-rock kimberlite compositions ($^{87}Sr/^{86}Sr_i$ of 0.70248–0.70464; $\varepsilon_{Nd(i)}$ of +1.2 to +3.9; data from Nelson, 1989; Gaffney et al., 2007; Tappe et al., 2011a). In agreement with many other perovskite Sr isotope studies (e.g., Paton et al., 2007; Woodhead et al., 2009), the perovskite Sr isotopic range is greatly restricted compared with the whole-rock kimberlite data and falls near the unradiogenic end of the observed $^{87}Sr/^{86}Sr$ spectrum. In contrast, there is complete overlap in the Nd isotope compositions between the Sarfartoq perovskites and the corresponding whole-rock kimberlites. The compositional range over slightly more than 2 epsilon Nd units thus appears to be a primary mantle signature and will be discussed in Sections 5.2. and 5.3. In this context it is important to note that the relatively large perovskite grain size of Sarfartoq kimberlites (50–200 μm) compared to those of perovskites from the majority of worldwide kimberlites (typically <100 μm) indicates near-liquidus crystallization, which makes a record of possible late-stage crustal contamination highly unlikely (cf., Malarkey et al., 2010). We furthermore note that the measured $^{87}Sr/^{86}Sr$ ratios of the perovskite fractions studied here are considered representative of the initial Sr isotopic composition, because Rb does not occupy perovskite lattice sites (Mitchell, 2002). Although the presence of up to 4 ppm Rb has been reported from kimberlitic perovskite (Yang et al., 2009), this Rb must occur as nanoinclusions or other forms of impurities (Roger Mitchell, personal communication 2012). Hence, radiogenic Sr derived from the decay of such 'non-structural' Rb will be readily removed during acid leaching as part of the cleaning procedure prior to TIMS analytical work (see Section 3.2.). This is evident from the negligibly low $^{87}Rb/^{86}Sr$ (<0.0005) of kimberlitic perovskites that were analyzed by conventional ID-TIMS (Heaman, 1989). Regardless, even the most elevated $^{87}Rb/^{86}Sr$ of ~0.02 reported for kimberlitic perovskite (Malarkey et al., 2010) only results in corrections for radiogenic in-growth of the measured $^{87}Sr/^{86}Sr$ on the 5th decimal place, which is within the analytical uncertainty of our measurements (Table 2).

The 158–166 Ma old kimberlite dykes at Tikiusaaq contain perovskites that show relatively restricted $^{87}Sr/^{86}Sr$ ranging between 0.70319 and 0.70346. The range of initial ε_{Nd} for these perovskite fractions is even more restricted, between +4.8 and +5.1. The

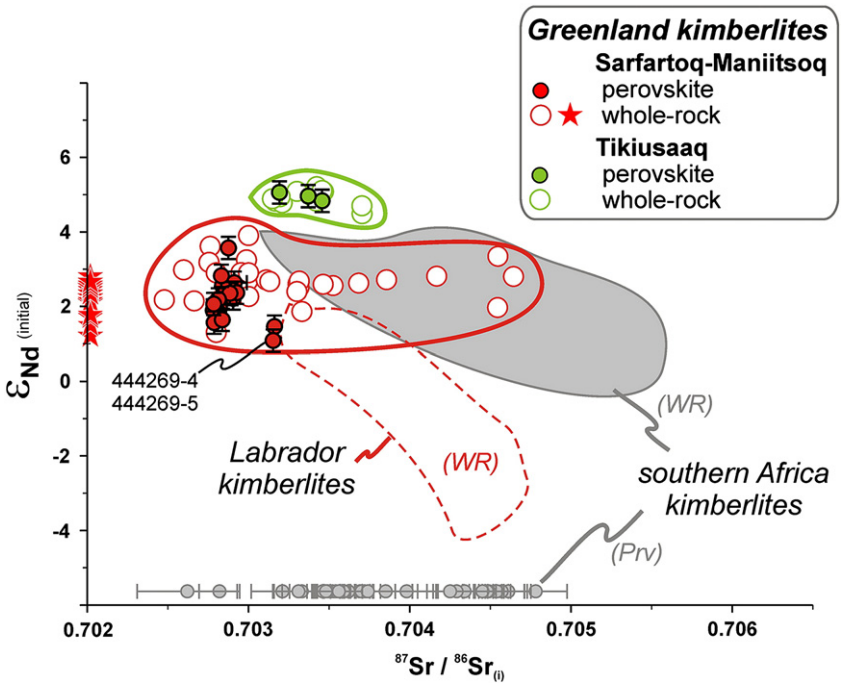

Fig. 4. $\varepsilon_{Nd(i)}$ vs. $^{87}Sr/^{86}Sr_i$ for perovskite from Greenland kimberlites. The new data for perovskites from the Neoproterozoic Sarfartoq (red) and Jurassic Tikiusaaq (green) kimberlite fields are superimposed over the respective whole-rock analyses (Nelson, 1989; Tappe et al., 2011a, unpublished). Solid red stars represent whole-rock Nd isotope data for Sarfartoq kimberlites from Gaffney et al. (2007). Also shown are compositional fields for whole-rock (WR) kimberlites from Labrador (Tappe et al., 2006, 2008) and Group-I kimberlites from southern Africa (Nowell et al., 2004). Solid gray circles represent Sr isotope compositions of perovskites (Prv) from Group-I kimberlites of southern Africa (Woodhead et al., 2009). All error bars are at the 2-sigma level of uncertainty. See main text for more details.

analyzed perovskites from Tikiusaaq nearly fully overlap their respective whole-rock kimberlite compositions ($^{87}Sr/^{86}Sr_i$ of 0.70315–0.70370; $\varepsilon_{Nd(i)}$ of +4.5 to +5.2; first author's unpublished data) in Sr–Nd isotope space (Fig. 4).

5. Age and origin of West Greenland kimberlites

5.1. Relationships between kimberlite and carbonatite magmatism

5.1.1. Temporal links

Regardless of whether there exists a petrogenetic relationship between kimberlites and carbonatites (Mitchell, 2005), the close spatial association of these distinct volatile-rich magma types in West Greenland cannot be ignored. This is particularly relevant for the Sarfartoq and Tikiusaaq kimberlite fields, where existing age data demonstrate a temporal link with the carbonatite magmatism that occurred in the same areas (Larsen et al., 1983; Larsen and Rex, 1992; Hutchison and Frei, 2009; Secher et al., 2009; Tappe et al., 2009, 2011a). We further improved these age constraints and our new high-precision U–Pb perovskite data allow for a more detailed assessment of the timing of kimberlite and carbonatite magmatic activities in West Greenland (Fig. 3).

At Sarfartoq, kimberlite dykes record a protracted history of CO_2-rich magma generation beneath the margin of the NAC between 590 and 550 Ma (Fig. 3A). The currently most precise date for the Sarfartoq carbonatite intrusion falls within the kimberlite age range at 572.8 ± 3.8 Ma (Tappe et al., 2011a). Although it is likely that this compositionally diverse carbonatite body formed during repeated magmatic pulses over a longer period of time than is recorded by the above cited single age, it is safe to conclude that kimberlite and carbonatite magmatism at Sarfartoq was coeval. Moreover, in terms of relative timing of magma emplacement, the now available data clearly indicate that carbonatite magmatism was pre- and post-dated by kimberlite eruptions. This detail has not been very clear from field relations alone, which point to an earlier emplacement of the kimberlite magma (Larsen and Rex, 1992). The petrogenetic significance of these new age data remains, of course, open to speculation, but it becomes clearer that overly simplistic models linking carbonatite and kimberlite intrusives by an increasing degree of partial melting (e.g., Dalton and Presnall, 1998; Agashev et al., 2008) are unsupported at Sarfartoq. In this context it should be noted that Dalton and Presnall (1998) had suggested that the Sarfartoq complex represents the best natural analog for their experimentally produced 'primary carbonatitic–kimberlitic melt continuum' at 6 GPa. With this in mind, we now evaluate the Jurassic intrusive history at Tikiusaaq in the central part of the NAC (Fig. 1).

Our refined U–Pb perovskite ages for Tikiusaaq kimberlites (~166–158 Ma) and the previously published age range of ~160–155 Ma for the associated carbonatite intrusion (Tappe et al., 2009; only the TIMS data are considered here) suggest onset of kimberlite magmatic activity some 6 Myr prior to carbonatite magmatism (Fig. 3B). The new age constraints furthermore suggest overlapping kimberlite and carbonatite magmatic activity, similar to the situation at Sarfartoq approximately 200 km north. However, unlike the timing of magmatism at Sarfartoq, there is at present no evidence from the Tikiusaaq area for kimberlitic magmatic activity post-dating carbonatite emplacement. If true, then this observation clearly argues against a 'primary carbonatitic–kimberlitic melt continuum' at Tikiusaaq, and alternative petrological mechanisms must be invoked to explain the prominent association of kimberlite and carbonatite magmatism in West Greenland.

5.1.2. Carbonatite magma evolution from kimberlitic parent melts

The scarcity of carbonatites at Earth's surface relative to typically associated silicate magmas is commonly explained by their highly reactive nature leading to interaction with peridotite in the mantle lithosphere during ascent (Dalton and Wood, 1993; Moore and Wood, 1998). However, this filtering effect cannot account for the intrusive history at Sarfartoq and Tikiusaaq, because hybrid carbonate–silicate magmas such as kimberlites (as opposed to pure silicate melts) are in

theory equally reactive with peridotite (Wyllie, 1980). If correct, and taking the higher viscosity of kimberlitic magmas compared with carbonate melts into account, then one would expect that kimberlites are even less likely to reach the surface (Moore and Wood, 1998; Sleep, 2009). However, Russell et al. (2012) have recently argued that kimberlitic magmas ascend ultrafast due to assimilation-fuelled buoyancy, and we briefly discuss this idea in light of the West Greenland occurrences in Section 5.1.3.

Based on the fact that coeval kimberlites and carbonatites at Sarfartoq share a moderately depleted Nd–Hf isotope signature (Tappe et al., 2011a), it appears that both magma types are derived from the same mantle source region and, thus, have a linked formation. Tappe et al. (2011a) rejected a primary melting relationship between carbonatites and kimberlites at Sarfartoq on the basis of several geochemical arguments. These include the more evolved carbon isotope composition of the carbonatite (−3.2‰ $\delta^{13}C_{PDB}$) compared with kimberlitic carbonates (−5.3 to −4‰ $\delta^{13}C_{PDB}$). Also, the relatively late emplacement of the carbonatite magma some 20 Myr after initiation of kimberlite magmatism does not support a model in which the carbonatite intrusion represents the first lowest-degree partial melt of carbonated peridotite in a continuum of 'primary carbonatitic–kimberlitic melt compositions' (cf., Dalton and Presnall, 1998; Gudfinnsson and Presnall, 2005; Brey et al., 2008). Based on compositional arguments presented before (Tappe et al., 2011a), we envisage the separation of a carbonate-rich melt fraction from hybrid carbonate–silicate magmas as the most viable mechanism that gave rise to the formation of the Sarfartoq carbonatite. On a smaller scale, operation of such a separation mechanism is evident from the presence of residual carbonatite veins in many of the West Greenland kimberlite dykes. Brooker (1998) demonstrated experimentally that carbonatite liquids can separate from hybrid carbonate–silicate magmas under CO_2 saturated conditions in the shallow cratonic mantle at 2.5 GPa. Unfortunately, many variables that control these separation processes such as bulk composition remain unconstrained. Tappe et al. (2006) suggested that removal of liquidus olivine and phlogopite (found as cumulates in kimberlitic rocks throughout the NAC) from rising carbonate–silicate magmas under uppermost mantle conditions (~1–2 GPa) must lead to CO_2 saturation of the residual liquids and in extreme cases cause carbonatite magma segregation. However, given the apparent scarcity of carbonatite intrusions that are associated with kimberlite fields (Woolley and Kjarsgaard, 2008), we have strong reason to believe that any such separation mechanism only rarely occurs in nature. We also conclude that carbonatite emplacement as part of a kimberlite province appears to be a rather random phenomenon, and as such, it is unlikely that any specific age pattern exists in relation to the accompanying kimberlite magmatism.

5.1.3. Carbonatite magma escape from ultra-depleted cratonic mantle

We have argued above that the carbonatites emplaced at crustal levels show compositional features suggestive of crystallization from rather evolved magmas, which were most likely derived from kimberlitic parent melts. Conversely, Nielsen and Sand (2008) demonstrated that the parental melts to the Greenland kimberlites were 'carbonatitic' as constrained by geochemical modeling. This highlights the possibility that carbonate-rich melt fractions can exist at various stages in kimberlite magmatic systems (Mitchell, 2005) and it is our intention here to elucidate that the carbonate-rich precursor melts to the Greenland kimberlites are not represented by the carbonatite bodies at crustal levels.

There exists increasing petrological evidence that kimberlitic magmas have carbonate melt precursors in the sublithospheric mantle. Their evolution to hybrid carbonate–silicate magmas of kimberlitic affinity is thought to occur by resorption of orthopyroxene during carbonate melt ascent through the cratonic mantle lithosphere (Mitchell, 2008; Kamenetsky et al., 2009; Russell et al., 2012). The attractiveness of this model lies in its ability to explain the restriction of kimberlites to cratons (Russell et al., 2012). Cratons are typically characterized by a mantle lithosphere that is not only thicker but also enriched in orthopyroxene compared with non-cratonic mantle lithosphere (Boyd, 1989; McDonough, 1990; Griffin et al., 2009). Cratonic mantle therefore provides ample opportunity for rising sublithospheric carbonate melts to react with orthopyroxene, a process that successively converts these primitive carbonate melts into kimberlitic magmas. Based on the fact that CO_2 solubility in carbonate melt drops with increasing MgO and SiO_2 contents, the reacting kimberlitic magmas begin to exsolve a CO_2 phase and are now enabled to erupt to the surface by their assimilation-driven buoyancy (Russell et al., 2012). However, the cratonic mantle beneath West Greenland is the most orthopyroxene-poor among studied mantle lithosphere worldwide, and this feature has been demonstrated to be a result of extensive mantle melting in Archean subduction zones (Bernstein et al., 2007; Pearson and Wittig, 2008). This observation raises the question of whether there is a link between the ultra-depleted nature of the NAC mantle lithosphere and the high abundance of cratonic carbonatites in West Greenland, which is much higher than seen in any other kimberlite province (Woolley and Kjarsgaard, 2008; Secher et al., 2009; Tappe et al., 2009).

It is tempting to speculate that a substantial amount of rising kimberlitic magmas beneath West Greenland remained relatively SiO_2-poor and enriched in carbonate component due to a limited opportunity to react with orthopyroxene within the deeper NAC mantle lithosphere. These less buoyant, 'delayed' kimberlitic magma batches (cf., Russell et al., 2012) must have been prone to the fractionation of significant amounts of olivine and phlogopite upon arrival at shallow mantle levels (cf., Tappe et al., 2006). It may have been such a pronounced removal of these – and possibly other – non-carbonate liquidus phases that promoted formation and separation of residual carbonatite liquids at shallow mantle levels (see Section 5.1.2.), which ultimately gave rise to the intrusion of sizeable carbonatite magma bodies into the crust. Regardless of the exact mode of carbonatite magma formation, the important point is that shallow ultra-depleted cratonic mantle certainly provided a favorable environment for such residual carbonatite liquids to escape, because decarbonation reactions are unlikely to occur in the absence of orthopyroxene (Dalton and Wood, 1993).

5.2. Constraints on the ultimate kimberlite magma source region

The origin of kimberlitic magmas is a controversial topic and many recently proposed models invoke exotic source components that reside as deep in the Earth's mantle as the transition zone or even the lower mantle (Bizzarro et al., 2002; Nowell et al., 2004; Gaffney et al., 2007; Paton et al., 2009). Most of the evidence for such an ultra-deep kimberlite origin is based on Nd–Hf isotope systematics that fall significantly below the terrestrial array. However, Tappe et al. (2011a) demonstrated that such displaced Nd–Hf isotope systematics can equally well be explained by small amounts of melt (<10%) from metasomatic components mixed into ascending convective mantle-derived melts (see Section 5.3.). In other words, there appears to be no need for involvement of ultra-deep components in the genesis of Group-I kimberlite magmas, which is in keeping with their rather normal, moderately depleted Sr and Nd isotope compositions on a worldwide basis (e.g., Smith, 1983).

The fact that kimberlite magmatism was recurrent over a ~40 Myr time span in the Sarfartoq area reveals that the Earth's mantle beneath West Greenland was able to sustain extraction of CO_2-rich melts for a prolonged period of time (Fig. 3A). In the Sarfartoq area there are no discernible differences in the Sr–Nd isotopic compositions and U–Pb perovskite ages between kimberlites from on- and off-craton localities (Fig. 1), which hint at magma derivation from beneath the ~200 km thick diamond-bearing lithosphere at 590–550 Ma (Sand et al., 2009). This observation corroborates the absence of differences in whole-rock kimberlite Nd–Hf isotope compositions between samples

taken from either side of the Nagssugtoqidian deformation front (Gaffney et al., 2007; Tappe et al., 2011a), which is widely considered to demarcate the boundary of the NAC (Kalsbeek et al., 1987). However, recently published Re–Os isotope systematics of peridotite xenoliths suggest a northward continuation of Archean cratonic mantle underneath the Paleoproterozoic Nagssugtoqidian mobile belt (Wittig et al., 2010).

Sleep (2009) recently suggested that the deep continental lithospheric mantle may represent a major carbonate reservoir that contains up to half the mass of CO_2 estimated to reside in the convecting mantle. The author envisaged the stored carbonate of the deep continental mantle lithosphere to have accumulated from failed CO_2-rich low-degree melts over the past 2 billion years. It is beyond the scope of this paper to assess whether such a carbonate reservoir indeed exists in the cratonic mantle, but it is important to point out that carbonate stored in the lithosphere for several hundred million years is an implausible source material for global kimberlite and carbonatite magmatism, because the radiogenic isotope signatures of these CO_2-rich magmas do not reveal long-term enrichment (Bizimis et al., 2003; Bell and Simonetti, 2010; Tappe et al., 2011a).

Mantle plumes or hotspots have frequently been proposed as sources for kimberlites and carbonatites (Le Roex, 1986; Haggerty, 1994; Ernst and Bell, 2010), but these rising columns of hot, solid material originating from the transition zone or lower mantle appear to be unlikely sources of the CO_2-rich magmatism across the NAC. For example, plate motion over a stationary hotspot for ~40 Myr should have resulted in a kimberlite corridor with resolvable age progression in West Greenland. However, we only observe a random age distribution of kimberlite intrusives in the Sarfartoq area, which are scattered along the Nagssugtoqidian deformation front, a major crustal suture zone (Fig. 1). Furthermore, plume-related magmatism typically shows a noticeable change in composition through time (Campbell, 2005), with the escape of an incipient carbonate-rich melt component being either restricted to the earliest plume stage (Dixon et al., 2008; Hofmann et al., 2011) or to the cooler plume periphery (Ernst and Bell, 2010). As none of these diagnostic hotspot patterns are observed at Sarfartoq or elsewhere in the NAC, we propose that the kimberlite and associated carbonatite magmas were ultimately derived from the convecting upper mantle. Mass balance constraints on the deep cycling of carbon also suggest that the relatively well-stirred convecting upper mantle may be the only mantle reservoir that would have the capacity to supply CO_2-rich melts over such a long time span (Dasgupta and Hirschmann, 2010). This is in keeping with the fairly uniform, depleted radiogenic isotope compositions of the kimberlitic perovskites from Sarfartoq (Fig. 4).

Improved understanding of the redox conditions in the Earth's mantle predicts that carbonate-bearing melts are only stable above ~250 km depth, because the mantle is metal saturated below this level (Stagno and Frost, 2010; Rohrbach and Schmidt, 2011). The diamondiferous kimberlites at Sarfartoq and Tikiusaaq entrained material from the base of the lithospheric mantle, with the deepest analyzed xenoliths having last equilibrated at ~200 and ~150 km depth, respectively (Sand et al., 2009; Tappe et al., 2011b). It therefore appears that the extraction of carbonate-bearing proto-kimberlitic melts beneath West Greenland was confined to a relatively narrow zone in the uppermost convecting mantle beneath a thick lid of cratonic lithosphere. Melt generation under these geodynamic conditions may be predominately controlled by redox reactions and does not require large temperature change (Foley, 2011). In particular, the oxidation of upwelling mantle material above ~250 km depth causes a notable depression of the peridotite solidus due to conversion of reduced C–H–O volatiles to H_2O and CO_2 (Wyllie, 1980; Green et al., 1987; Foley, 2011). Carbonate-rich melts produced near the solidus of upper mantle peridotite by such a redox melting mechanism sample disproportionately large amounts of convectively remixed heterogeneities (Hirschmann, 2010). This may help to explain the only moderate levels of depletion in the Sr and Nd isotope compositions of kimberlitic perovskites from West Greenland

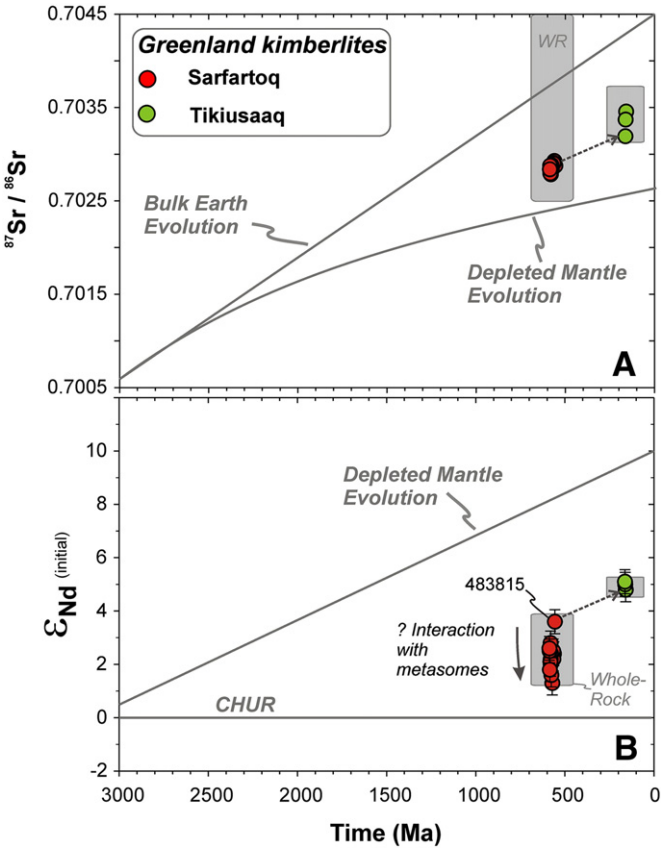

Fig. 5. Initial Sr (A) and Nd (B) isotope compositions of perovskites from Greenland kimberlites in isotope evolution diagrams. The underlying parameters for the various evolution curves are summarized in Table 1 of Workman and Hart (2005). The Depleted MORB Mantle evolution is calculated here for continuous depletion since 3 Ga based on the assumption that crust–mantle differentiation before that time was negligible (see details in Workman and Hart, 2005). Perovskites from kimberlite sample 444269 are not shown, because their Sr–Nd isotope systematics is interpreted to record pronounced interaction with an enriched metasomatic component (see Fig. 4). The dashed arrows indicate an inferred isotopic evolution of a common convective upper mantle source region for Neoproterozoic Sarfartoq and Mesozoic Tikiusaaq kimberlites beneath the NAC. Error bars are at the 2-sigma level of uncertainty, and are smaller than symbol size for $^{87}Sr/^{86}Sr_i$ ratios. CHUR — Chondritic Uniform Reservoir.

(Figs. 4–5), and in general the similarity between the radiogenic isotope signatures of global kimberlites/carbonatites and OIBs (Smith, 1983; Nelson et al., 1988; Carlson et al., 2006; Bell and Simonetti, 2010).

An important implication of our model is that small volumes of carbonate-rich *or* proto-kimberlitic melt may always be present at the base of the cratonic lithosphere. Local concentration of these carbonate-rich melts during mantle flow along the rugged underside of the thick cratonic lithosphere (Rabinowicz et al., 2002; Gregoire et al., 2006), together with marked changes in the lithospheric stress field (Jelsma et al., 2009), may be the most important factors in controlling the spatial and temporal distribution of kimberlite eruptions at Earth's surface. Because the topology of the underside of the cratonic lithosphere undergoes frequent change (O'Reilly et al., 2001; Tappe et al., 2007; Foley, 2008; Eaton et al., 2009), it would be a natural consequence that kimberlite magmatism shifts position across a craton through time, as observed in West Greenland (Fig. 8).

5.3. Remobilization of cratonic metasomes

Despite the overall homogeneity of the perovskite Sr and Nd isotope compositions from Sarfartoq kimberlites, we note that perovskites from kimberlite dyke 444269 have Sr and Nd isotope compositions suggesting involvement of a long-term enriched source material (Fig. 4). This sample falls between the majority of the Sarfartoq kimberlites and the

600–555 Ma old kimberlites from Labrador, which define a pronounced enrichment trend in Sr–Nd isotope space. In an attempt to explain the origin of Labrador kimberlites, Tappe et al. (2008) suggested an interaction process between carbonate-rich melt from the convecting upper mantle and old MARID-type metasomes at the base of the cratonic lithosphere (the MARID suite of xenoliths was originally described as mica–amphibole–rutile–ilmenite–diopside-bearing; Dawson and Smith, 1977). This model has been extended to West Greenland (Nielsen et al., 2009), where the shift toward slightly lower $^{176}Hf/^{177}Hf$ ratios of Sarfartoq kimberlites relative to their coeval on-craton analogs from Maniitsoq (Figs. 1 and 8) was explained by <5% melt contribution from phlogopite-rich metasomes to passing carbonate-rich melts from the convecting upper mantle (Tappe et al., 2011a). Hafnium isotopes were demonstrated to be the most sensitive monitor of this mixing process due to extremely high Hf concentration levels in MARID-type metasomes, whereas the Nd and in particular Sr elemental budgets are largely controlled by the carbonate-rich melt component derived from the convecting upper mantle. In this regard it is also important to bear the relatively high compatibility of Sr in phlogopite and K-richterite during partial fusion of MARID-type metasomes in mind (Foley et al., 1996; Tiepolo et al., 2003). Note, however, the apparently opposing conclusion in Paton et al. (2009), where it was inferred that high Sr concentration levels of the cratonic mantle (mineralogy not specified) exert strong control on the Sr isotope compositions of passing kimberlitic melts from below the lithosphere. In any case, the subtle enrichment seen in the Sr–Nd isotope systematics of perovskites from Sarfartoq kimberlite 444269 may be an expression of a similar interaction process between carbonate-rich melts and old metasomes. Re–Os isotope evidence for metasomatic overprinting of the deep mantle lithosphere beneath Sarfartoq at ~2.0 Ga (Wittig et al., 2010), and the increasing abundance of phlogopite-bearing peridotite xenoliths toward and across the craton margin (Larsen and Garrit, 2005), further substantiate that such an interaction process may indeed have occurred during kimberlite magma formation. Although little is known about the distribution of phlogopite-rich metasomes at the NAC base, we infer their presence to be highly irregular, most likely in the form of vein networks. Such metasomatic vein networks preferentially form along zones of lithospheric weakness, that is, along ancient suture zones and craton margins (Vaughan and Scarrow, 2003; Tappe et al., 2007; Foley, 2008). Within the context of an asthenosphere–lithosphere interaction model, it is interesting to note that at the northern NAC margin the youngest known kimberlite dyke (483815; 556.7 ± 2.6 Ma) records the most depleted Nd isotope signal ($\varepsilon_{Nd(i)} = +3.6$; Fig. 5B), although associated with the largest analytical uncertainty in our data set. This may suggest that large parts of the isotopically enriched component (?metasomatic veins) had already been consumed in melting reactions during the preceding deep magmatic events from below the cratonic lithosphere.

Unfortunately, there are only three perovskite samples available from the Jurassic Tikiusaaq kimberlite dykes in the central part of the NAC. Their Nd isotope compositions are extremely homogenous and highly radiogenic ($\varepsilon_{Nd(i)}$ of +4.8 to +5.1), suggestive of magma derivation from the convecting upper mantle, with little or no involvement of readily fusible phlogopite-rich metasomes. Therefore, we only consider these largely unmodified Tikiusaaq samples, together with the isotopically most depleted samples from Sarfartoq, in our discussion of the Sr–Nd isotope evolution of the ultimate kimberlite magma source region beneath the NAC (Fig. 5). Such an approach is common practice in the study of the origin of continental flood basalt magmatism (Carlson et al., 2006), and should be equally appropriate for tracking the sublithospheric kimberlite magma sources.

5.4. The sublithospheric kimberlite magma source through time

Our new combined U–Pb, Sr, and Nd isotope data for perovskites from Neoproterozoic and Mesozoic kimberlites in West Greenland

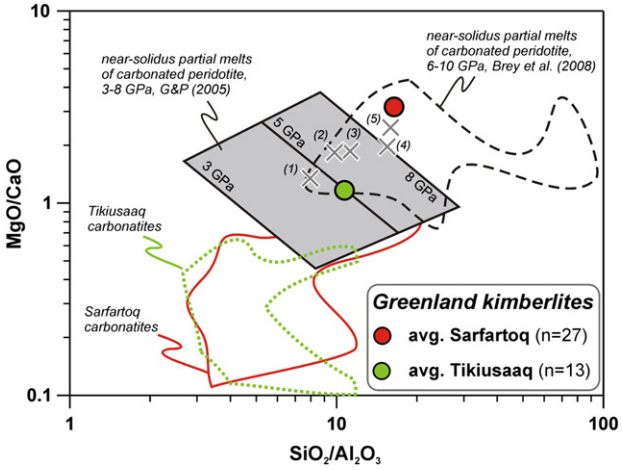

Fig. 6. MgO/CaO vs. SiO_2/Al_2O_3 for average kimberlite (see Table 3), as well as range of carbonatite compositions from Sarfartoq (Gaffney et al., 2007; Tappe et al., 2011a) and Tikiusaaq (Steenfelt et al., 2007). Fields for experimentally produced melt compositions from synthetic and natural carbonated peridotites under high pressures are after Gudfinnsson and Presnall (2005) and Brey et al. (2008), respectively. Gray crosses are reconstructed parent kimberlite magma compositions from (1) — the Majuagaa kimberlite dyke, West Greenland; (2) — South African Group-I kimberlite; (3) — Lac de Gras kimberlite, Canada; (4) — Jericho kimberlite, Canada; (5) — Udachnaya East kimberlite, Russia (see compilation in Kjarsgaard et al., 2009). Note the higher Mg/Ca and Si/Al ratios of Sarfartoq kimberlites compared with their Tikiusaaq analogs, which may indicate melt generation at slightly higher pressures (see model in Fig. 8). Note further the almost complete overlap between carbonatite compositions from the Sarfartoq and Tikiusaaq kimberlite fields in West Greenland. A compilation of the high-quality major element analyses used for the calculation of average Sarfartoq and Tikiusaaq kimberlite compositions is given in Table A (Supplementary data file).

provide the opportunity to track the mantle source region beneath the NAC through time (Fig. 5). Before we engage in this exercise, we shall reiterate that both the Sarfartoq and Tikiusaaq kimberlites are diamondiferous and must be derived from depths exceeding ~150 km. We furthermore note their strong similarity in terms of mineralogical (Nielsen et al., 2009; Tappe et al., 2009) and geochemical composition (Figs. 6–7; Steenfelt et al., 2007), as well as their association with sizeable carbonatite intrusions (Figs. 1 and 8). Based on these primary observations, we assume that the Sarfartoq and Tikiusaaq kimberlite magmas formed from similar mantle material (i.e., peridotite plus H_2O- and CO_2-rich fluid) under conditions that must have been quite reproducible (Figs. 6–7). If correct, then it follows from the distinctly different $^{87}Sr/^{86}Sr_{(i)}$ and $^{143}Nd/^{144}Nd_{(i)}$ ratios of kimberlitic perovskites (Figs. 4–5) that either the source material experienced a

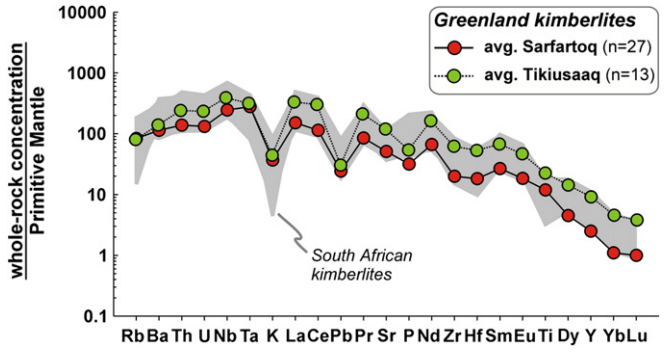

Fig. 7. Primitive Mantle normalized incompatible element distribution for average kimberlite from the Sarfartoq (Gaffney et al., 2007; Tappe et al., 2011a) and Tikiusaaq (Steenfelt et al., 2007) fields. Note the overall similarity of the kimberlite patterns from West Greenland, and their close match with South African Group-I kimberlite trace element compositions (Le Roex et al., 2003). Primitive Mantle values are from Palme and O'Neill (2003). A compilation of the high-quality trace element analyses used for the calculation of average Sarfartoq and Tikiusaaq kimberlite compositions is given in Table A (Supplementary data file).

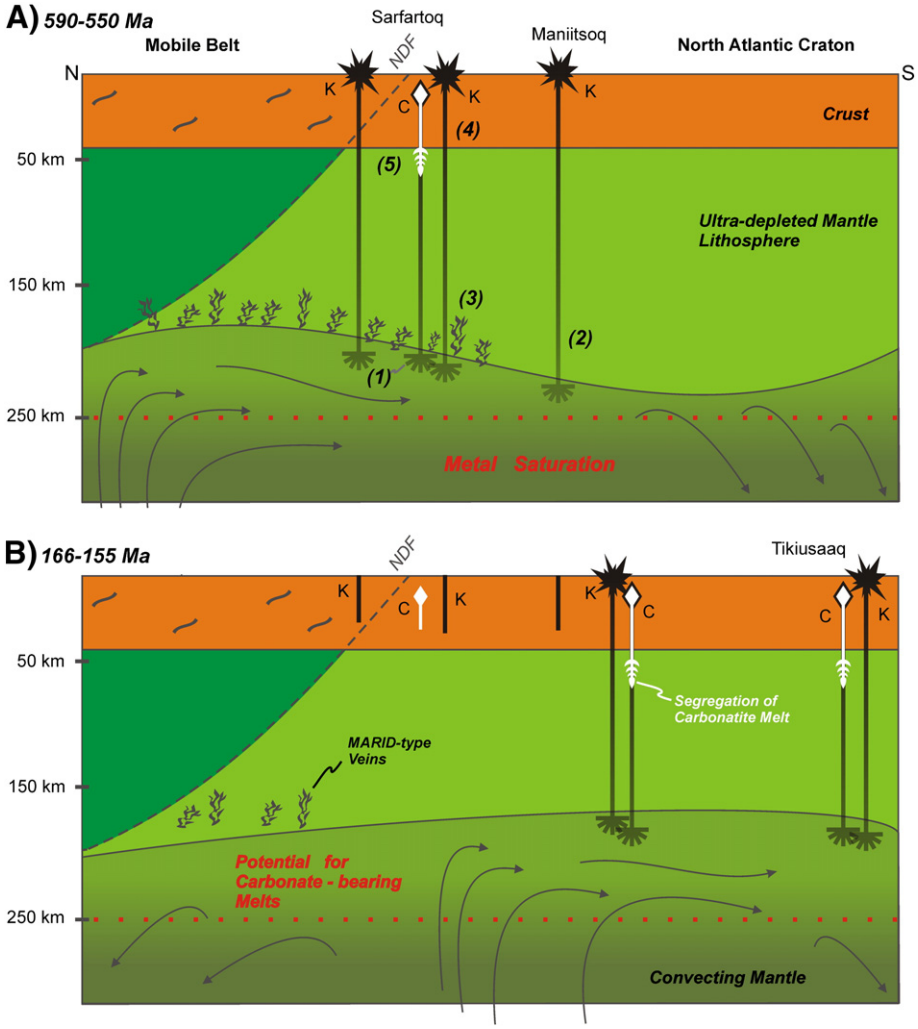

Fig. 8. Model of kimberlite (K) and carbonatite (C) magma formations beneath the North Atlantic craton of West Greenland through time. (A) Neoproterozoic kimberlite and associated carbonatite magmatism occurred at the craton margin in the Sarfartoq area between ~590 and 550 Ma. (B) Mesozoic kimberlite and carbonatite magmatic activities occurred in the craton interior between ~200 and 150 Ma (e.g., ~166–155 Ma at Tikiusaaq). Our favored explanation for this geographic shift of kimberlite/carbonatite magmatism is a changing topology of the craton base with accompanying changes in the small-scale mantle flow patterns due to progressive lithosphere stretching and thinning. Note that the ultimate kimberlite magma source region is the upwelling mantle directly beneath >150 km thick cratonic lithosphere during both the Neoproterozoic (A) and Mesozoic (B). However, differences in the depth of kimberlite magma formation through time are most likely controlled by lithosphere thickness variations. The model includes the following petrogenetic details: (*1*) Local concentration of carbonate-rich near-solidus melts due to compaction during mantle flow along the underside of thick cratonic lithosphere. Note that such carbonate melts may always be present within the zone between ~250 km depth and the lithosphere base, but these low-viscosity melts rarely pool. Note further that below 250 km depth the stability of carbonate-bearing melts is greatly restricted due to metal saturation in the deeper mantle (Rohrbach and Schmidt, 2011). (*2*) If the stress field allows, then carbonate-rich proto-kimberlitic melts can percolate through the base of the cratonic lithosphere and react with orthopyroxene (Russell et al., 2012). This process successively converts the carbonate melts into carbonate–silicate magmas of kimberlitic affinity (note the gradation from light gray to black). (*3*) In the vicinity of the craton margin, the rising carbonate-rich melts may encounter MARID-type metasomes, which can impart distinctive enriched geochemical flavors to the convecting mantle-derived proto-kimberlite magmas. (*4*) While some kimberlite magma batches ascend directly through the cratonic mantle lithosphere by assimilation-fuelled buoyancy (Russell et al., 2012), (*5*) other kimberlitic magma batches did not digest sufficient orthopyroxene to be able to erupt to the surface. These 'delayed' carbonate–silicate magmas may separate residual carbonatite liquids within the shallow ultra-depleted mantle lithosphere, which are now enabled to intrude the cratonic crust. NDF — Nagssugtoqidian Deformation Front.

different time-integrated Rb/Sr and Sm/Nd history (i.e., two distinct mantle reservoirs) or, as we will argue below, the source material is simply the same isotopically evolving convective upper mantle (Fig. 8).

In Fig. 5 it is evident that the higher $^{87}Sr/^{86}Sr_{(i)}$ and $^{143}Nd/^{144}Nd_{(i)}$ of the Mesozoic kimberlites (Tikiusaaq) compared with their Neoproterozoic counterparts (Sarfartoq) may simply be a function of isotope evolution of the same mantle reservoir, because the apparent slope along which radiogenic in-growth may have occurred (dashed arrows) approaches that of Bulk Earth evolution. In detail, however, we note that the level to which the Mesozoic kimberlites record more radiogenic Sr and Nd isotope compositions is somewhat intermediate between Bulk Earth (Primitive Mantle) and Depleted MORB Mantle evolution models (Workman and Hart, 2005). The source Rb/Sr and Sm/Nd ratios required to link Neoproterozoic and Mesozoic kimberlite magmas from West Greenland to a common isotopically evolving mantle reservoir are approximately 0.025 and 0.35, respectively (Fig. 5). Again, these parent/daughter element ratios are intermediate between Bulk Earth (Rb/Sr of 0.0307 and Sm/Nd of 0.325) and Depleted MORB Mantle (Rb/Sr of 0.0065 and Sm/Nd of 0.411; see compilation in Workman and Hart, 2005), but extremely different from deep NAC mantle lithosphere (Rb/Sr of 0.08 ± 0.04 and Sm/Nd of 0.17 ± 0.04; Wittig et al., 2008). From this we infer that the putative common kimberlite source region has a memory of mantle depletion throughout much of the Phanerozoic, that is, it has participated in global crust–mantle differentiation. Hence, the convecting upper mantle appears to be the most plausible reservoir from which Neoproterozoic and Mesozoic kimberlite magmas beneath the NAC originated. This model does not, however, preclude the involvement of recycled crustal components in the genesis of kimberlites. It simply predicts that the isotopic fingerprint of

any such convectively remixed component will be less extreme (see modified FOZO concept of Stracke et al., 2005) compared to models that invoke long-term storage of recycled oceanic crust in isolated mantle regions such as the transition zone (Ringwood et al., 1992; Nowell et al., 2004). Furthermore, the redox-controlled incipient melting regime that is prevalent within the convecting upper mantle directly beneath thick cratonic lithosphere (see Section 5.2.) almost certainly 'oversamples' recycled components due to their generally lower melting points (Sobolev et al., 2007). This geodynamic scenario beneath cratons therefore partly resembles what is widely known as 'lid effect' in oceanic intra-plate settings, where OIBs erupted on thick lithosphere tend to show pronounced geochemical and isotopic enrichment (Prytulak and Elliott, 2007; Niu et al., 2011). In this context, it is important to reiterate the well-known fact that high-quality Sr–Nd isotope data of worldwide Group-I kimberlites and their megacrysts typically fall within the oceanic mantle array (Mahotkin et al., 2000; Davies et al., 2001; Nowell et al., 2004; Carlson et al., 2006; Kopylova et al., 2009; Yang et al., 2009). This reinforces our isotopic argument that there is no a priori reason to resort to ultra-deep and compositionally extreme mantle sources in the genesis of kimberlite magmas, as also pointed out by Kramers et al. (1981) on geochemical grounds.

6. Summary and conclusion

1. The West Greenland kimberlite province comprises Neoproterozoic (e.g., Sarfartoq) and Mesozoic (e.g., Tikiusaaq) kimberlites and associated intrusive carbonatites. Based on our perovskite multi-isotope study, together with published results from experimental petrology, we suggest that the kimberlitic magmas were ultimately derived from the convecting upper mantle directly beneath the root of the North Atlantic craton. At the craton margin in the Sarfartoq area, however, elevated Nd isotope variability of both the perovskites and corresponding whole-rock kimberlites is observed. The trend toward isotopic enrichment recorded by Sarfartoq perovskites is interpreted in terms of interaction between rising carbonate-rich melts from the asthenosphere with cratonic mantle lithosphere. However, our data currently do not allow for a more detailed assessment of whether the lithospheric component was derived from partial fusion of cratonic metasomes or, alternatively, from the assimilation of peridotitic orthopyroxene, or perhaps from both.
2. We explain the geographic shift of kimberlite and associated carbonatite magmatic activity from the craton margin during the Neoproterozoic toward the craton center during the Mesozoic by changes in localized, small-scale mantle flow along the underside of progressively thinning cratonic lithosphere.
3. In agreement with many perovskite isotope studies that utilize LA–MC-ICP-MS analysis, it appears that perovskite is a reliable archive of near-primary Sr and Nd isotope information in kimberlite magmatic systems. We confirm the more robust nature of Sr isotope data from perovskite compared to corresponding bulk kimberlite analyses, which typically contain records of alteration and/or crustal contamination. However, we find that, contrary to common belief, the Nd isotope compositions of bulk kimberlites may fingerprint the mantle source(s) with equal reliability to the corresponding Nd isotope data from perovskites.

Supplementary data to this article can be found online at http://dx.doi.org/10.1016/j.chemgeo.2012.05.026.

Acknowledgments

This work is published with permission from the Geological Survey of Denmark and Greenland. ST was partly supported by the Humboldt Foundation during the course of this project. We are indebted to Karsten Secher for the advice during the early stages of this project and for resurrecting the interest in the timing of kimberlite magmatism in West Greenland. Andreas Stracke, Rolf Romer, James LeBlanc, Andy DuFrane, Katie Smart, Joshua Davies, and Dima Kamenetsky are gratefully acknowledged for their helpful discussions that ensued during the course of this study. Journal reviews by Amy Gaffney and Chad Paton, as well as advice from editor Laurie Reisberg hopefully improved the clarity of our argumentation.

References

Agashev, A.M., Pokhilenko, N.P., Takazawa, E., McDonald, J.A., Vavilov, M.A., Watanabe, T., Sobolev, N.V., 2008. Primary melting sequence of a deep (>250 km) lithospheric mantle as recorded in the geochemistry of kimberlite–carbonatite assemblages, Snap Lake dyke system, Canada. Chemical Geology 255, 317–328.
Batumike, J.M., Griffin, W.L., Belousova, E.A., Pearson, N.J., O'Reilly, S.Y., Shee, S.R., 2008. LAM-ICPMS U–Pb dating of kimberlitic perovskite: Eocene–Oligocene kimberlites from the Kundelungu Plateau, D.R. Congo. Earth and Planetary Science Letters 267, 609–619.
Bell, K., Simonetti, A., 2010. Source of parental melts to carbonatites: critical isotopic constraints. Mineralogy and Petrology 98, 77–89.
Bernstein, S., Kelemen, P.B., Hanghøj, K., 2007. Consistent olivine Mg# in cratonic mantle reflects Archean mantle melting to the exhaustion of orthopyroxene. Geology 35, 459–462.
Bizimis, M., Salters, V.J.M., Dawson, J.B., 2003. The brevity of carbonatite sources in the mantle: evidence from Hf isotopes. Contributions to Mineralogy and Petrology 145, 281–300.
Bizzarro, M., Simonetti, A., Stevenson, R.K., David, J., 2002. Hf isotope evidence for a hidden mantle reservoir. Geology 30, 771–774.
Boyd, F.R., 1989. Compositional distinction between oceanic and cratonic lithosphere. Earth and Planetary Science Letters 96, 15–26.
Brey, G.P., Bulatov, V.K., Girnis, A.V., Lahaye, Y., 2008. Experimental melting of carbonated peridotite at 6–10 GPa. Journal of Petrology 49, 797–821.
Brooker, R.A., 1998. The effect of CO_2 saturation on immiscibility between silicate and carbonate liquids: an experimental study. Journal of Petrology 39, 1905–1915.
Campbell, I.H., 2005. Large igneous provinces and the mantle plume hypothesis. Elements 1, 265–269.
Carlson, R.W., Czamanske, G., Fedorenko, V., Ilupin, I., 2006. A comparison of Siberian meimechites and kimberlites: implications for the source of high-Mg alkalic magmas and flood basalts. Geochemistry, Geophysics, Geosystems 7, Q11014.
Chalmers, J.A., Pulvertaft, T.C.R., 2001. Development of the continental margins of the Labrador Sea: a review. In: Wilson, R.C.L., Whitmarsh, R.B., Taylor, B., Froitzheim, N. (Eds.), Non-volcanic Rifting of Continental Margins: a Comparison of Evidence from Land and Sea. Geological Society of London, London, United Kingdom, pp. 77–105.
Corfu, F., Dahlgren, S., 2008. Perovskite U–Pb ages and the Pb isotopic composition of alkaline volcanism initiating the Permo-Carboniferous Oslo Rift. Earth and Planetary Science Letters 265, 256–269.
Currie, C.A., Beaumont, C., 2011. Are diamond-bearing Cretaceous kimberlites related to low-angle subduction beneath western North America? Earth and Planetary Science Letters 303, 59–70.
Dalton, J.A., Presnall, D.C., 1998. The continuum of primary carbonatitic-kimberlitic melt compositions in equilibrium with lherzolite: data from the system CaO–MgO–Al_2O_3–SiO_2–CO_2 at 6 GPa. Journal of Petrology 39, 1953–1964.
Dalton, J.A., Wood, B.J., 1993. The compositions of primary carbonate melts and their evolution through wallrock reaction in the mantle. Earth and Planetary Science Letters 119, 511–525.
Dasgupta, R., Hirschmann, M.M., 2010. The deep carbon cycle and melting in Earth's interior. Earth and Planetary Science Letters 298, 1–13.
Davies, G.R., Spriggs, A.J., Nixon, P.H., 2001. A non-cognate origin for the Gibeon kimberlite megacryst suite, Namibia: implications for the origin of Namibian kimberlites. Journal of Petrology 42, 159–172.
Dawson, J.B., Smith, J.V., 1977. The MARID (mica–amphibole–rutile–ilmenite–diopside) suite of xenoliths in kimberlite. Geochimica et Cosmochimica Acta 41, 309–323.
Dixon, J., Clague, D.A., Cousens, B., Monsalve, M.L., Uhl, J., 2008. Carbonatite and silicate melt metasomatism of the mantle surrounding the Hawaiian plume: evidence from volatiles, trace elements, and radiogenic isotopes in rejuvenated-stage lavas from Niihau, Hawaii. Geochemistry, Geophysics, Geosystems 9, Q09005.
Eaton, D.W., Darbyshire, F., Evans, R.L., Grütter, H., Jones, A.G., Yuan, X.H., 2009. The elusive lithosphere–asthenosphere boundary (LAB) beneath cratons. Lithos 109, 1–22.
Ernst, R.E., Bell, K., 2010. Large igneous provinces (LIPs) and carbonatites. Mineralogy and Petrology 98, 55–76.
Foley, S.F., 2008. Rejuvenation and erosion of the cratonic lithosphere. Nature Geoscience 1, 503–510.
Foley, S.F., 2011. A reappraisal of redox melting in the Earth's mantle as a function of tectonic setting and time. Journal of Petrology 52, 1363–1391.
Foley, S.F., Jackson, S.E., Fryer, B.J., Greenough, J.D., Jenner, G.A., 1996. Trace element partition coefficients for clinopyroxene and phlogopite in an alkaline lamprophyre from Newfoundland by LAM-ICP-MS. Geochimica et Cosmochimica Acta 60, 629–638.
Gaffney, A.M., Blichert-Toft, J., Nelson, B.K., Bizzarro, M., Rosing, M., Albarede, F., 2007. Constraints on source-forming processes of West Greenland kimberlites inferred from Hf–Nd isotope systematics. Geochimica et Cosmochimica Acta 71, 2820–2836.
Gibson, S.A., Thompson, R.N., Day, J.A., 2006. Timescales and mechanisms of plume–lithosphere interactions: $^{40}Ar/^{39}Ar$ geochronology and geochemistry of alkaline

igneous rocks from the Parana–Etendeka large igneous province. Earth and Planetary Science Letters 251, 1–17.
Goldstein, S.L., O'Nions, R.K., Hamilton, P.J., 1984. A Sm–Nd isotopic study of atmospheric dusts and particulates from major river systems. Earth and Planetary Science Letters 70, 221–236.
Green, D.H., Falloon, T.J., Taylor, W.R., 1987. Mantle-derived magmas: roles of variable source peridotite and variable C–H–O fluid compositions. In: Mysen, B.O. (Ed.), Magmatic Processes: Physicochemical Principles. Geochemical Society, University Park, United States, pp. 139–154.
Gregoire, M., Rabinowicz, M., Janse, A.J.A., 2006. Mantle mush compaction: a key to understand the mechanisms of concentration of kimberlite melts and initiation of swarms of kimberlite dykes. Journal of Petrology 47, 631–646.
Griffin, W.L., O'Reilly, S.Y., Afonso, J.C., Begg, G.C., 2009. The composition and evolution of lithospheric mantle: a re-evaluation and its tectonic implications. Journal of Petrology 50, 1185–1204.
Gudfinnsson, G.H., Presnall, D.C., 2005. Continuous gradations among primary carbonatitic, kimberlitic, melilititic, basaltic, picritic, and komatiitic melts in equilibrium with garnet lherzolite at 3–8 GPa. Journal of Petrology 46, 1645–1659.
Haggerty, S.E., 1994. Superkimberlites: a geodynamic diamond window to the Earth's core. Earth and Planetary Science Letters 122, 57–69.
Hansen, K., 1980. Lamprophyres and carbonatitic lamprophyres related to rifting in the Labrador Sea. Lithos 13, 145–152.
Heaman, L.M., 1989. The nature of the subcontinental mantle from Sr–Nd–Pb isotopic studies on kimberlitic perovskite. Earth and Planetary Science Letters 92, 323–334.
Hirschmann, M.M., 2010. Partial melt in the oceanic low velocity zone. Physics of the Earth and Planetary Interiors 179, 60–71.
Hofmann, A.W., Farnetani, C.G., Spiegelman, M., Class, C., 2011. Displaced helium and carbon in the Hawaiian plume. Earth and Planetary Science Letters 312, 226–236.
Hutchison, M.T., Frei, D., 2009. Kimberlite and related rocks from Garnet Lake, West Greenland, including their mantle constituents, diamond occurrence, age and provenance. Lithos 112, 318–333.
Hutchison, M.T., Nielsen, L.J., Bernstein, S., 2007. P–T history of kimberlite-hosted garnet lherzolites from South–West Greenland. Geological Survey of Denmark and Greenland Bulletin 13, 45–48.
Jacobsen, S.B., Wasserburg, G.J., 1980. Sm–Nd isotopic evolution of chondrites. Earth and Planetary Science Letters 50, 139–155.
Jelsma, H., Barnett, W., Richards, S., Lister, G., 2009. Tectonic setting of kimberlites. Lithos 112, 155–165.
Kalsbeek, F., Pidgeon, R.T., Taylor, P.N., 1987. Nagssugtoqidian mobile belt of West Greenland: a cryptic 1850 Ma suture between two Archaean continents — chemical and isotopic evidence. Earth and Planetary Science Letters 85, 365–385.
Kamenetsky, V.S., Kamenetsky, M.B., Sobolev, A.V., Golovin, A.V., Sharygin, V.V., Pokhilenko, N.P., Sobolev, N.V., 2009. Can pyroxenes be liquidus minerals in the kimberlite magma? Lithos 112, 213–222.
Keen, C.E., Dickie, K., Dehler, S.A., 2012. The volcanic margins of the northern Labrador Sea: insights to the rifting process. Tectonics 31, TC1011.
Kjarsgaard, B.A., Pearson, D.G., Tappe, S., Nowell, G.M., Dowall, D., 2009. Geochemistry of hypabyssal kimberlites from Lac de Gras, Canada: comparisons to a global database and applications to the parent magma problem. Lithos 112, 236–248.
Kopylova, M.G., Nowell, G.M., Pearson, D.G., Markovic, G., 2009. Crystallization of megacrysts from protokimberlitic fluids: geochemical evidence from high-Cr megacrysts in the Jericho kimberlite. Lithos 112, 284–295.
Kramers, J.D., Smith, C.B., 1983. A feasibility study of U–Pb and Pb–Pb dating of kimberlites using groundmass mineral fractions and whole-rock samples. Chemical Geology 41, 23–38.
Kramers, J.D., Smith, C.B., Lock, N.P., Harmon, R.S., Boyd, F.R., 1981. Can kimberlites be generated from an ordinary mantle. Nature 291, 53–56.
Larsen, L.M., Garrit, D., 2005. Mapping of the lithosphere beneath the Archaean craton and Proterozoic mobile belt in West Greenland. Report — Geological Survey of Denmark and Greenland 68, 55–56.
Larsen, L.M., Rex, D.C., 1992. A review of the 2500 Ma span of alkaline-ultramafic, potassic and carbonatitic magmatism in West Greenland. Lithos 28, 367–402.
Larsen, L.M., Rex, D.C., Secher, K., 1983. The age of carbonatites, kimberlites and lamprophyres from southern West Greenland: recurrent alkaline magmatism during 2500 million years. Lithos 16, 215–221.
Larsen, L.M., Heaman, L.M., Creaser, R.A., Duncan, R.A., Frei, R., Hutchison, M., 2009. Tectonomagmatic events during stretching and basin formation in the Labrador Sea and the Davis Strait: evidence from age and composition of Mesozoic to Palaeogene dyke swarms in West Greenland. Journal of the Geological Society 166, 999–1012.
Le Roex, A.P., 1986. Geochemical correlation between southern African kimberlites and South-Atlantic hotspots. Nature 324, 243–245.
Le Roex, A.P., Bell, D.R., Davis, P., 2003. Petrogenesis of Group I kimberlites from Kimberley, South Africa: evidence from bulk-rock geochemistry. Journal of Petrology 44, 2261–2286.
Ludwig, K.R., 2000. Isoplot/Ex version 2.2. — a geochronological toolkit for Microsoft Excel. Berkeley Geochronology Center Special Publication No. 1a Berkeley, California.
Lugmair, G.W., Marti, K., 1978. Lunar initial $^{143}Nd/^{144}Nd$: differential evolution of the lunar crust and mantle. Earth and Planetary Science Letters 39, 349–357.
Mahotkin, I.L., Gibson, S.A., Thompson, R.N., Zhuravlev, D.Z., Zherdev, P.U., 2000. Late Devonian diamondiferous kimberlite and alkaline picrite (proto-kimberlite?) magmatism in the Arkhangelsk region, NW Russia. Journal of Petrology 41, 201–227.
Malarkey, J., Pearson, D.G., Kjarsgaard, B.A., Davidson, J.P., Nowell, G.M., Ottley, C.J., Stammer, J., 2010. From source to crust: tracing magmatic evolution in a kimberlite and a melilitite using microsample geochemistry. Earth and Planetary Science Letters 299, 80–90.
McDonough, W.F., 1990. Constraints on the composition of the continental lithospheric mantle. Earth and Planetary Science Letters 101, 1–18.
Mitchell, R.H., 2002. Perovskites: Modern and Ancient. Almaz Press, Thunder Bay. 249 pp.
Mitchell, R.H., 2005. Carbonatites and carbonatites and carbonatites. The Canadian Mineralogist 43, 2049–2068.
Mitchell, R.H., 2008. Petrology of hypabyssal kimberlites: relevance to primary magma compositions. Journal of Volcanology and Geothermal Research 174, 1–8.
Moore, K.R., Wood, B.J., 1998. The transition from carbonate to silicate melts in the $CaO–MgO–SiO_2–CO_2$ system. Journal of Petrology 39, 1943–1951.
Nelson, D.R., 1989. Isotopic characteristics and petrogenesis of the lamproites and kimberlites of central West Greenland. Lithos 22, 265–274.
Nelson, D.R., Chivas, A.R., Chappell, B.W., McCulloch, M.T., 1988. Geochemical and isotopic systematics in carbonatites and implications for the evolution of ocean–island sources. Geochimica et Cosmochimica Acta 52, 1–17.
Nielsen, T.F.D., Sand, K.K., 2008. The Majuagaa kimberlite dike, Maniitsoq region, West Greenland: constraints on an Mg-rich silicocarbonatitic melt composition from groundmass mineralogy and bulk compositions. The Canadian Mineralogist 46, 1043–1061.
Nielsen, T.F.D., Jensen, S.M., Secher, K., Sand, K.K., 2009. Distribution of kimberlite and aillikite in the Diamond Province of southern West Greenland: a regional perspective based on groundmass mineral chemistry and bulk compositions. Lithos 112, 358–371.
Niu, Y.L., Wilson, M., Humphreys, E.R., O'Hara, M.J., 2011. The origin of intra-plate ocean island basalts (OIB): the lid effect and its geodynamic implications. Journal of Petrology 52, 1443–1468.
Nowell, G.M., Pearson, D.G., Bell, D.R., Carlson, R.W., Smith, C.B., Kempton, P.D., Noble, S.R., 2004. Hf isotope systematics of kimberlites and their megacrysts: new constraints on their source regions. Journal of Petrology 45, 1583–1612.
O'Reilly, S.Y., Griffin, W.L., Djomani, Y.H., Morgan, P., 2001. Are lithospheres forever? Tracking changes in subcontinental lithospheric mantle through time. GSA Today 11, 4–10.
Palme, H., O'Neill, H.S.C., 2003. Cosmochemical estimates of mantle composition. In: Carlson, R.W. (Ed.), Treatise on Geochemistry. Elsevier, Amsterdam, pp. 1–38.
Paton, C., Hergt, J.M., Phillips, D., Woodhead, J.D., Shee, S.R., 2007. New insights into the genesis of Indian kimberlites from the Dharwar craton via in situ Sr isotope analysis of groundmass perovskite. Geology 35, 1011–1014.
Paton, C., Hergt, J.M., Woodhead, J.D., Phillips, D., Shee, S.R., 2009. Identifying the asthenospheric component of kimberlite magmas from the Dharwar craton, India. Lithos 112, 296–310.
Pearce, J.A., Peate, D.W., 1995. Tectonic implications of the composition of volcanic arc magmas. Annual Review of Earth and Planetary Sciences 23, 251–285.
Pearson, D.G., Wittig, N., 2008. Formation of Archaean continental lithosphere and its diamonds: the root of the problem. Journal of the Geological Society 165, 895–914.
Prytulak, J., Elliott, T., 2007. TiO_2 enrichment in ocean island basalts. Earth and Planetary Science Letters 263, 388–403.
Rabinowicz, M., Ricard, Y., Gregoire, M., 2002. Compaction in a mantle with a very small melt concentration: implications for the generation of carbonatitic and carbonate-bearing high alkaline mafic melt impregnations. Earth and Planetary Science Letters 203, 205–220.
Rao, N.V.C., Lehmann, B., 2011. Kimberlites, flood basalts and mantle plumes: new insights from the Deccan large igneous province. Earth-Science Reviews 107, 315–324.
Ringwood, A.E., Kesson, S.E., Hibberson, W.O., Ware, N., 1992. Origin of kimberlites and related magmas. Earth and Planetary Science Letters 113, 521–538.
Rohrbach, A., Schmidt, M.W., 2011. Redox freezing and melting in the Earth's deep mantle resulting from carbon–iron redox coupling. Nature 472, 209–212.
Russell, J.K., Porritt, L.A., Lavallee, Y., Dingwell, D.B., 2012. Kimberlite ascent by assimilation-fuelled buoyancy. Nature 481, 352–357.
Sand, K.K., Waight, T.E., Pearson, D.G., Nielsen, T.F.D., Makovicky, E., Hutchison, M.T., 2009. The lithospheric mantle below southern West Greenland: a geothermobarometric approach to diamond potential and mantle stratigraphy. Lithos 112, 1155–1166.
Secher, K., Heaman, L.M., Nielsen, T.F.D., Jensen, S.M., Schjøth, F., Creaser, R.A., 2009. Timing of kimberlite, carbonatite, and ultramafic lamprophyre emplacement in the alkaline province located 64°–67°N in southern West Greenland. Lithos 112, 400–406.
Sharp, W.E., 1974. A plate tectonic origin for diamond-bearing kimberlites. Earth and Planetary Science Letters 21, 351–354.
Sleep, N.H., 2009. Stagnant lid convection and carbonate metasomatism of the deep continental lithosphere. Geochemistry, Geophysics, Geosystems 10, Q11010.
Smith, C.B., 1983. Pb, Sr and Nd isotopic evidence for sources of southern African Cretaceous kimberlites. Nature 304, 51–54.
Sobolev, A.V., Hofmann, A.W., Kuzmin, D.V., Yaxley, G.M., Arndt, N.T., Chung, S.L., Danyushevsky, L.V., Elliott, T., Frey, F.A., Garcia, M.O., Gurenko, A.A., Kamenetsky, V.S., Kerr, A.C., Krivolutskaya, N.A., Matvienkov, V.V., Nikogosian, I.K., Rocholl, A., Sigurdsson, I.A., Sushchevskaya, N.M., Teklay, M., 2007. The amount of recycled crust in sources of mantle-derived melts. Science 316, 412–417.
Stacey, J.S., Kramers, J.D., 1975. Approximation of terrestrial lead isotope evolution by a two-stage model. Earth and Planetary Science Letters 26, 207–221.
Stagno, V., Frost, D.J., 2010. Carbon speciation in the asthenosphere: experimental measurements of the redox conditions at which carbonate-bearing melts coexist with graphite or diamond in peridotite assemblages. Earth and Planetary Science Letters 300, 72–84.
Steenfelt, A., Schjøth, F., Sand, K.K., Secher, K., Tappe, S., Moberg, E., Tukiainen, T., 2007. Initial assessment of the geology and economic potential of the Tikiusaaq carbonatite complex and ultramafic lamprophyre dykes. Report — Geological Survey of Denmark and Greenland 2007 (64), 1–53.
Steiger, R.H., Jäger, E., 1977. Subcommission on geochronology: convention on the use of decay constants in geo- and cosmochronology. Earth and Planetary Science Letters 36, 359–362.

Stracke, A., Hofmann, A.W., Hart, S.R., 2005. FOZO, HIMU, and the rest of the mantle zoo. Geochemistry, Geophysics, Geosystems 6, Q05007.
Tachibana, Y., Kaneoka, I., Gaffney, A., Upton, B.G.J., 2006. Ocean–island basalt-like source of kimberlite magmas from West Greenland revealed by high $^{3}He/^{4}He$ ratios. Geology 34, 273–276.
Tanaka, T., Togashi, S., Kamioka, H., Amakawa, H., Kagami, H., Hamamoto, T., Yuhara, M., Orihashi, Y., Yoneda, S., Shimizu, H., Kunimaru, T., Takahashi, K., Yanagi, T., Nakano, T., Fujimaki, H., Shinjo, R., Asahara, Y., Tanimizu, M., Dragusanu, C., 2000. JNdi-1: a neodymium isotopic reference in consistency with La Jolla neodymium. Chemical Geology 168, 279–281.
Tappe, S., Simonetti, A., 2012. Combined U–Pb geochronology and Sr–Nd isotope analysis of the Ice River perovskite standard, with implications for kimberlite and alkaline rock petrogenesis. Chemical Geology 304–305, 10–17.
Tappe, S., Foley, S.F., Jenner, G.A., Heaman, L.M., Kjarsgaard, B.A., Romer, R.L., Stracke, A., Joyce, N., Hoefs, J., 2006. Genesis of ultramafic lamprophyres and carbonatites at Aillik Bay, Labrador: a consequence of incipient lithospheric thinning beneath the North Atlantic craton. Journal of Petrology 47, 1261–1315.
Tappe, S., Foley, S.F., Stracke, A., Romer, R.L., Kjarsgaard, B.A., Heaman, L.M., Joyce, N., 2007. Craton reactivation on the Labrador Sea margins: $^{40}Ar/^{39}Ar$ age and Sr–Nd–Hf–Pb isotope constraints from alkaline and carbonatite intrusives. Earth and Planetary Science Letters 256, 433–454.
Tappe, S., Foley, S.F., Kjarsgaard, B.A., Romer, R.L., Heaman, L.M., Stracke, A., Jenner, G.A., 2008. Between carbonatite and lamproite — diamondiferous Torngat ultramafic lamprophyres formed by carbonate-fluxed melting of cratonic MARID-type metasomes. Geochimica et Cosmochimica Acta 72, 3258–3286.
Tappe, S., Steenfelt, A., Heaman, L.M., Simonetti, A., 2009. The newly discovered Jurassic Tikiusaaq carbonatite – aillikite occurrence, West Greenland, and some remarks on carbonatite–kimberlite relationships. Lithos 112, 385–399.
Tappe, S., Pearson, D.G., Nowell, G.M., Nielsen, T.F.D., Milstead, P., Muehlenbachs, K., 2011a. A fresh isotopic look at Greenland kimberlites: cratonic mantle lithosphere imprint on deep source signal. Earth and Planetary Science Letters 305, 235–248.
Tappe, S., Smart, K.A., Pearson, D.G., Steenfelt, A., Simonetti, A., 2011b. Craton formation in Late Archean subduction zones revealed by first Greenland eclogites. Geology 39, 1103–1106.
Thirlwall, M.F., 1991. Long-term reproducibility of multicollector Sr and Nd isotope ratio analysis. Chemical Geology 94, 85–104.
Tiepolo, M., Zanetti, A., Oberti, R., Brumm, R., Foley, S.F., Vannucci, R., 2003. Trace-element partitioning between synthetic potassic-richterites and silicate melts, and contrasts with the partitioning behaviour of pargasites and kaersutites. European Journal of Mineralogy 15, 329–340.
Torsvik, T.H., Burke, K., Steinberger, B., Webb, S.J., Ashwal, L.D., 2010. Diamonds sampled by plumes from the core–mantle boundary. Nature 466, 352–355.
Vaughan, A.P.M., Scarrow, J.H., 2003. K-rich mantle metasomatism control of localization and initiation of lithospheric strike–slip faulting. Terra Nova 15, 163–169.
Wittig, N., Pearson, D.G., Webb, M., Ottley, C.J., Irvine, G.J., Kopylova, M., Jensen, S.M., Nowell, G.M., 2008. Origin of cratonic lithospheric mantle roots: a geochemical study of peridotites from the North Atlantic craton, West Greenland. Earth and Planetary Science Letters 274, 24–33.
Wittig, N., Webb, M., Pearson, D.G., Dale, C.W., Ottley, C.J., Hutchison, M., Jensen, S.M., Luguet, A., 2010. Formation of the North Atlantic craton: timing and mechanisms constrained from Re–Os isotope and PGE data of peridotite xenoliths from SW Greenland. Chemical Geology 276, 166–187.
Woodhead, J., Hergt, J., Phillips, D., Paton, C., 2009. African kimberlites revisited: in situ Sr-isotope analysis of groundmass perovskite. Lithos 112, 311–317.
Woolley, A.R., Kjarsgaard, B.A., 2008. Paragenetic types of carbonatite as indicated by the diversity and relative abundances of associated silicate rocks: evidence from a global database. The Canadian Mineralogist 46, 741–752.
Workman, R.K., Hart, S.R., 2005. Major and trace element composition of the depleted MORB mantle (DMM). Earth and Planetary Science Letters 231, 53–72.
Wu, F.Y., Yang, Y.H., Mitchell, R.H., Li, Q.L., Yang, J.H., Zhang, Y.B., 2010. In situ U–Pb age determination and Nd isotopic analysis of perovskites from kimberlites in southern Africa and Somerset Island, Canada. Lithos 115, 205–222.
Wyllie, P.J., 1980. The origin of kimberlite. Journal of Geophysical Research 85, 6902–6910.
Yang, Y.H., Wu, F.Y., Wilde, S.A., Liu, X.M., Zhang, Y.B., Xie, L.W., Yang, J.H., 2009. In situ perovskite Sr–Nd isotopic constraints on the petrogenesis of the Ordovician Mengyin kimberlites in the North China Craton. Chemical Geology 264, 24–42.